



저작자표시-비영리-변경금지 2.0 대한민국

이용자는 아래의 조건을 따르는 경우에 한하여 자유롭게

- 이 저작물을 복제, 배포, 전송, 전시, 공연 및 방송할 수 있습니다.

다음과 같은 조건을 따라야 합니다:



저작자표시. 귀하는 원저작자를 표시하여야 합니다.



비영리. 귀하는 이 저작물을 영리 목적으로 이용할 수 없습니다.



변경금지. 귀하는 이 저작물을 개작, 변형 또는 가공할 수 없습니다.

- 귀하는, 이 저작물의 재이용이나 배포의 경우, 이 저작물에 적용된 이용허락조건을 명확하게 나타내어야 합니다.
- 저작권자로부터 별도의 허가를 받으면 이러한 조건들은 적용되지 않습니다.

저작권법에 따른 이용자의 권리는 위의 내용에 의하여 영향을 받지 않습니다.

이것은 [이용허락규약\(Legal Code\)](#)을 이해하기 쉽게 요약한 것입니다.

[Disclaimer](#)

理學碩士 學位論文

분자선 에피택시법을 이용한 고품질 GaSb
박막성장에 관한 연구

Study on the growth of high quality GaSb films using Molecular Beam Epitaxy



2009年 2月

韓國海洋大學校 大學院

應用科學科 半導體物理專攻

李 雄



理學碩士 學位論文

분자선 에피탁시법을 이용한 고품질 GaSb
박막성장에 관한 연구

Study on the growth of high quality GaSb films using Molecular Beam Epitaxy

指導教授

金紅承



2008年 12月

韓國海洋大學校 大學院

應用科學科 半導體物理專攻

李 雄

本 論 文 을 李 雄 의 理 學 碩 士 學 位 論 文 으 로 認 准 함

위원장 양 민 (인)

위 원 김 홍 승 (인)

위 원 이 홍 찬 (인)



2008 년 12 월 24 일

한국해양대학교 대학원

Contents

Figure list.....	1
Table list.....	6
논문 요약.....	7
Abstract.....	9

Chapter 1. Introduction

1.1) Introduction to GaSb based materials

1.1.1) Physical properties of GaSb.....	11
---	----

1.1.2) Potential applications of GaSb.....	14
--	----

1.1.3) Research of GaSb heteroepitaxy and IR optoelectronic devices....	17
---	----

1.2) Current status of GaSb research

1.2.1) Problems in GaSb heteroepitaxy.....	24
--	----

1.2.2) Proposal of thesis.....	26
--------------------------------	----

1.3) Outline of thesis.....	27
-----------------------------	----

Reference.....	29
----------------	----

Chapter 2. Experiment

2.1) Epitaxy.....	32
-------------------	----

2.2) Three-types of epitaxial growth.....	33
---	----

2.3) Molecular beam epitaxy.....	35
----------------------------------	----

2.4) Reflection high energy electron diffraction (RHEED)	37
2.5) Atomic force microscopy.....	42
2.6) High resolution X-ray diffraction (HR-XRD)	
2.6.1) Conventional high resolution X-ray.....	44
2.6.2) ω scan (rocking curve) and ω -2 θ scan.....	46
2.7) Cathodoluminescence (CL).....	51
References.....	56

Chapter 3. Structural deformation reduction of MBE grown ZnTe by LT-buffer

3.1) Introduction.....	57
3.2) Experimental details.....	58
3.3) Initial growth observation	60
3.4) Surface morphology.....	62
3.5) The investigation of crystallinity.....	64
3.6) Crystal deformation.....	67
3.7) Conclusion.....	69
Reference.....	70

Chapter 4. MBE growth of GaSb films by using three-step ZnTe buffer layer

4.1) Introduction.....	72
4.2) Experiment details	73
4.3) Surface observation.....	75

4.4) Surface morphology.....	76
4.5) The crystallinity improvement.....	78
4.6) Structural deformation.....	80
4.7) Conclusion.....	83
Reference.....	84

Chapter 5. MBE growth of GaSb films ; The influence of the chemical composition of ZnTe surface

5.1) Introduction.....	86
5.2) Experimental details.....	86
5.3) The growth temperature optimization of growth.....	88
5.4) The RHEED observation by interface composition.....	91
5.5) Surface morphology.....	95
5.6) Evaluation of structural characterization by interface composition.....	96
5.7) Low temperature cathodoluminescence properties	99
5.8) Temperature dependence CL properties.....	101
5.9) Accelerating voltage dependence CL properties.....	104
5.10) Conclusion.....	107
References	109

Chapter 6. Summary and conclusion 112

Acknowledgements..... 114

Curriculum vitae..... 116



Figure list

Chapter 1

Figure 1.1 Crystal structure of GaSb zinc-blende

Figure 1.2 Band gap as a function of lattice constant for compound semiconductors

Figure 1.3 Applications of GaSb based compound semiconductors

Figure 1.4 (a) and (b) are X-ray ω - 2θ (004) rocking curves of GaSb grown without/with LT-GaSb nucleation layer, respectively

Figure 1.5 Avalanche photodetector structure of GaAlAsSb

Figure 1.6 Current-voltage characteristic of AlGaSb/GaSb avalanche photodiode.

Inset shows a cross-sectional view of avalanche photodiode.

Figure 1.7 optical absorption spectrum of GaSb at 4 and 300 K.

Chapter 2

Figure 2.1 Classification of epitaxy

Figure 2.2 Schematic representation of the three crystal growth modes. θ represents the coverage in monolayer.

Figure 2.3 Schematic illustration of molecular beam epitaxy system

Figure 2.4 Schematic illustration of RHEED observation

Figure 2.5 RHEED specular spot intensity

Figure 2.6 Schematic illustration of AFM

Figure 2.7 Schematic illustration of HRXRD geometry

Figure 2.8 Ewald sphere construction (for symmetric reflections, i.e. reflecting planes are parallel to the surface) for the ω - 2θ scan geometry. The bold arrow indicates the movement in the reciprocal lattice

Figure 2.9 Reciprocal space map showing accessible range for Bragg reflection measurement.



Figure 2.10 Diagram of generation and recombination of electron-hole pairs

Figure 2.11 Simulation of the scattered electrons by the Monte Carlo method

Figure 2.12 Correspondence between the electron range and the electron penetration

Chapter 3

Figure 3.1 The schematic drawing of prepared samples

Figure 3.2 RHEED images of (a) sample-A (HT-ZnTe/GaAs) and (b) sample-B (HT-ZnTe/LT-ZnTe/GaAs)

Figure 3.3 AFM images of (a) sample-A (HT-ZnTe/GaAs) and (b) sample-B (HT-ZnTe/LT-ZnTe/GaAs)

Figure 3.4 X-ray diffraction measurement results of (a) $\omega/\omega-2\Theta$ scan of sample-A (HT-ZnTe/GaAs) and (b) $\omega/\omega-2\Theta$ scan of sample-B (HT-ZnTe/LT-ZnTe/GaAs)

Figure 3.5 XRD reciprocal space mapping results of (a) sample-A (HT-ZnTe/GaAs) and (b) sample-B (HT-ZnTe/LT-ZnTe/GaAs)



Chapter 4

Figure 4.1 RHEED images of (a) sample-A (GaSb/GaAs) and (b) sample-B (GaSb/ZnTe buffer/GaAs)

Figure 4.2 AFM images of (a) sample-A and (b) sample-B

Figure 4.3 X-ray diffraction measurement results of (a) $\omega/\omega-2\Theta$ scan of sample-A and (b) $\omega/\omega-2\Theta$ scan of sample-B

Figure 4.4 X-ray diffraction reciprocal space mapping results of (a) sample-A

and (b) sample-B

Chapter 5

Figure 5.1 Growth temperature dependence of GaSb/GaAs layer. The surface roughness and HRXRD linewidth optimized at 525 °C.

Figure 5.2 RHEED patterns of sample-A (GaSb/Zn-terminated ZnTe) (a) c(2 x 2) Zn-terminated ZnTe surface, (b) initial growth of GaSb, (c) 0.4 mm GaSb; sample-B (GaSb/Te-terminated ZnTe) (d) (2 x 1) Te-terminated ZnTe surface, (e) initial growth of GaSb, (f) 0.4 mm GaSb. 3D growth was not observed from sample-A.

Figure 5.3 AFM images of (a) sample-A (GaSb/Zn-terminated ZnTe, RMS = 1.419 nm) and (b) sample-B (GaSb/Te-terminated ZnTe, RMS = 1.82 nm).

Figure 5.4 HR-XRD (004) ω -2 θ scan of (a) sample-A (GaSb/Zn-terminated ZnTe), (b) sample-B (GaSb/Te-terminated ZnTe) and (c) GaSb/GaAs.

Figure 5.5 Cathodoluminescence spectrum of GaSb/Zn-terminated ZnTe at 20 K. The inset is an energy diagram for the conduction band to neutral acceptor transition (eA_0)

Figure 5.6 (a) temperature dependence CL spectra and (b) activation energy of eA_0 emission.

Figure 5.7 Acceleration voltage dependence CL spectra



Table list

Table 1.1 Material properties of GaSb

Table 2.1 The effects of substrate and epilayer parameters upon the rocking curve

Table 5.1 Lattice constant, residual strain and relaxation ratio of GaSb layers grown on GaAs substrates with/without ZnTe buffer



논문 요약

본 논문에서는 III-V족 화합물 반도체인 GaSb 물질을 ZnTe 완화 층을 이용하여 이중접합구조로 제작하고 그것의 구조적, 광학적 조사를 통하여 고품질의 GaSb 박막 성장에 대한 가능성을 고찰하였다. 이 논문의 목적은 종래에 사용해 오던 기관과의 커다란 격차 부 정합 차에 의해 고품질의 성장이 제한이 되어온 GaSb 이중성장을 ZnTe 완화 층을 사용, 성장 조건의 최적화에 따라 얻은 고품질의 GaSb 박막의 새로운 성장 가능성을 보여줌에 있다. 본 논문은 총 7 장으로 구성되어 있으며 각 장의 내용은 다음과 같다.

제 1장에서는 기본적인 GaSb 물성과 종래의 GaSb 이중성장이 가지고 있는 문제점, 그리고 다양한 응용분야에 대하여 설명을 하였다. 제 2장에서는 제작된 GaSb 이중접합 구조를 성장, 평가하기 위해 본 연구에서 사용한 방법인, MBE, RHEED, AFM, XRD 그리고 CL 측정에 대하여 정리를 하였다. 제 3장은 낮은 온도에서 성장한 저온 ZnTe 버퍼를 사용하여 GaSb 성장 시 완화 층으로 사용되는 고품질의 ZnTe의 성장에 있다. 그리고 저온 완화 층을 이용하여 성장한 ZnTe의 구조적 특성

에 대해 고찰하였다. 제 4장에서는 3단계 ZnTe 완화 층을 이용하여 GaSb 박막을 성장 하였다. XRD 측정결과, ZnTe 버퍼에 의해 GaSb 구조적 변형 방지 및 GaSb 박막 질이 향상된 것을 알 수 있었다. 제 5장에서는 GaSb과 ZnTe 사이의 이종계면의 화학적 조성 변화에 의한 GaSb 성장의 최적화를 실시 하였다. 최적의 조건에서 성장된 GaSb 이종 접합 구조는 ZnTe 완화 층 표면의 Zn 처리에 의해 고품질의 박막 질을 구현시켰다. 또한 CL을 이용하여 성장한 GaSb 박막의 광 특성을 평가 하였다. 온도 변화 및 깊이 변화 CL 측정결과 GaSb과 ZnTe 버퍼 사이에 형성된 계면으로부터 발생하는 결함으로부터의 영향은 관찰되지 않았으며, 이것은 ZnTe 버퍼로 인해 고품질의 GaSb 박막의 성장의 가능성을 강력히 보여주었다. 마지막으로 제 6장에서는 본 논문에서 얻은 결과를 정리하여 결론 및 향후 과제에 대해 기술하였다.

Abstract

In this thesis, growth and structural and optical properties of GaSb with ZnTe buffer layer have been investigated. The objective of this thesis is to grow the high quality GaSb films by using ZnTe buffer layer according to the optimization of growth temperature and ZnTe buffer layer growth mechanism.

In the chapter 1, the fundamental GaSb properties, problems in the GaSb heteroepitaxy, and many applications of the GaSb heterostructure are introduced. In the chapter 2, the principles of molecular beam epitaxy (MBE), reflection high energy electron diffraction (RHEED), atomic force microscopy (AFM), high resolution X-ray diffraction (HR-XRD), and cathodoluminescence (CL) are explained. In the chapter 3, the role of the low temperature ZnTe buffer is systematically studied. The ZnTe films grown on low temperature ZnTe buffer are analyzed in terms of the structural properties. In the chapter 4, the high quality GaSb film growth is achieved by using three steps ZnTe buffer layer. XRD results show that the preventing of structural deformation and improvement of GaSb crystallinity are achieved by effects of ZnTe buffer layer. In the chapter 5, Zn-

terminated ZnTe surface for GaSb growth is selected for the GaSb growth to obtain high quality GaSb layers and the interface quality is proved in terms of structural properties and luminescence property. The results show that considerable features originated from the GaSb/ZnTe heterointerface has not been observed presumably due to high interface quality. This strongly supports the availability of ZnTe buffer for high quality GaSb growth.

Finally, the results found from this thesis are summarized and concluded in the chapter 6.



Chapter 1. Introduction

1.1) Introduction to GaSb based materials

1.1.1) Physical properties of GaSb

Among III-V compound semiconductors with narrow bandgap energy such as InAs, HgCdTe, InGaAs, GaSb and InSb, the GaSb is particularly an attractive material due to interested material properties as listed in table 1.1. The GaSb has a band gap 0.72 eV at room temperature (and 0.81 eV at 35 K) and a zinc-blend structure which is identical to the diamond lattice structure except each Ga atom has four tetrahedrally arranged Sb neighbours and vice versa as shown figure 1.1.

Table 1.1. Material properties of GaSb

Lattice constant (\AA)	6.095
Density (cm^{-3})	5.6137
Melting point (K)	985
Coefficient of thermal expansion at 300 K ($10^{-6} \text{ }^{\circ}\text{C}^{-1}$)	7.75
Thermal conductivity at 300 K ($\text{W cm}^{-1}\text{K}^{-1}$)	0.39
Direct energy gap at 300 K (eV)	0.72

Temperature dependence of minimum energy gap	4.2
Spin-orbit splitting energy, Δ_0 (eV)	0.80
Effective mass of electrons (in units of m_0)	0.041
Effective mass of heavy holes (in units of m_0)	0.28
Effective mass of light holes (in units of m_0)	0.05
Spin-orbit split mass	0.13
Wave number of LO phonons (cm^{-1})	233
Wave number of TO phonons (cm^{-1})	224
Refractive index (near band-gap energy)	3.82
Dielectric constant ϵ_0	15.69
Dielectric constant ϵ_∞	14.44



The melting point of GaSb is 712 °C [1] which is substantially lower than the 1240 °C of GaAs melting point. This can present processing problems, such as loss of Sb at moderate temperatures (the energy for dissociation is 10 ~ 14 Kcal/mol) [2], but the material is stable against oxidation by water vapour unlike (AlGa)Sb compounds of high Al content.

The undoped GaSb is always p-type with hole concentration of the order of 10^{16} cm^{-3} in nature irrespective of the growth technique and conditions. The native

defect responsible is Ga vacancies (V_{Ga}) and Ga in Sb site (Ga_{Sb}) [3]. The center is doubly ionized with the first and second levels lying 33 and 80 meV above the valence band edge [4]. It has also been suggested that Ga vacancy may be complex with Ga_{Sb} . To overcome this problem, study on epitaxial layers of GaSb grown by molecular beam epitaxy (MBE) with excess antimony [5] has shown the possibility of reducing substantially the level of nature acceptors and increasing the hole mobility. This stimulated the renewed interest in growth of GaSb crystals with reduced residual acceptors.

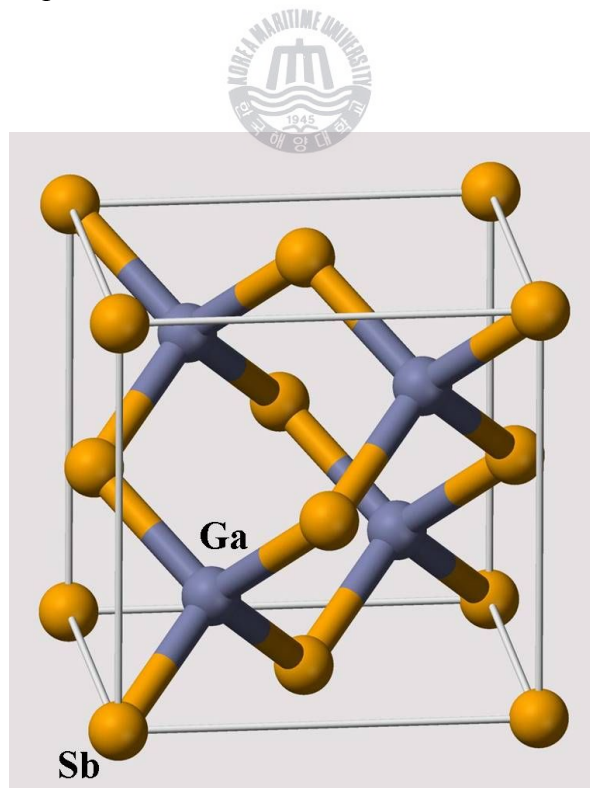


Figure 1.1 Crystal structure of GaSb zinc-blende

Figure 1.2 is a familiar diagram of energy gap vs lattice constants. GaSb is provided as a substrate material because its lattice parameter matches solid solutions of various ternary and quaternary III-V compounds whose band gaps cover a wide spectral range from ~ 0.3 to 1.58 eV, i.e., $0.8 \sim 4.3 \mu\text{m}$, as depicted figure 1.2 [2]. Also, detection of longer wavelengths, $8 \sim 14 \mu\text{m}$, is possible with intersubband absorption in Sb-based superlattices [6]. These studies have stimulated a lot of interest in GaSb for basic research as well as device fabrication.

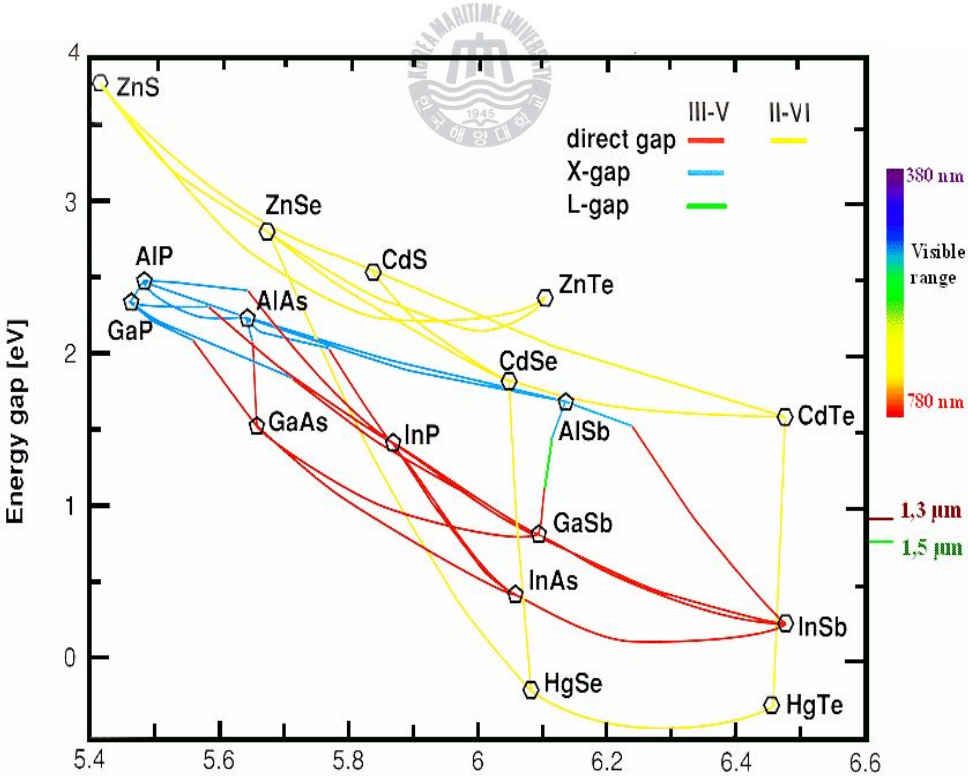


Figure 1.2 Band gap as a function of lattice constant for compound semiconductors

1.1.2) Potential applications of GaSb

GaSb-based structure have shown potentiality for applications in laser diodes with low threshold voltage [7,8], photodetectors with high quantum efficiency [9], high frequency devices [10,11], superlattices with optical and transport characteristics [12], booster cells in tandem solar cell arrangements for improved efficiency of photovoltaic cells and high efficiency thermophotovoltaic (TPV) cells [13]. Figure 1.3 describes these applications.



Figure 1.3 Applications of GaSb

Interestingly, the spin-orbit splitting of the valence band is almost equal to the energy band gap in GaSb leading to high hole ionization coefficients. This results in significant improvement in the signal-to-noise ratio at $\lambda > 1.3 \mu\text{m}$ in GaAlSb avalanche photodetectors grown on GaSb [9]. GaSb is also predicted to have the lattice mismatched electron mobility greater than GaAs making it of potential interest in the fabrication of microwave devices. Also, a ternary GaSb such InGaSb has been proposed as an ideal material for transferred-electron devices with low threshold yield and a large velocity peak-to-valley ratio, using a Monte Carlo simulation based on the three level model [11].



Especially, GaSb-based devices are promising candidates for a variety of military and civil applications in the $2 \sim 5 \mu\text{m}$ and $8 \sim 14 \mu\text{m}$ regimes: to mention a few, infrared (IR) imaging sensors for missile and surveillance system (focal plane arrays), fire detection and monitoring environmental pollution. The absorption wavelengths of several industrial gases and water vapour lie in the near IR range for which GaSb based alloys are suitable. Gas purity monitoring and trace moisture detection in corrosive gases like HCl in semiconductor processing, detecting micro leaks of toxic gases such as PH_3 , NOX, gases from automobile exhaust, in situ

monitoring of plasma etching, detecting hazardous gases like HF, H₂S in chemical plants, monitoring green house gas fluxes, measurements of flame species in microgravity combustion and humidity determination are a few areas where GaSb based alloys might find potential application. IR detector in 8 ~ 14 μm regime based on GaAlSb/AlSb and InAs/InGaSb superlattices and InAsSb are believed to be potential competitors for the present day HgCdTe detectors [14].

1.1.3) Research of GaSb heteroepitaxy and IR optoelectronic devices

At an early time, GaSb epitaxy has been largely carried out by liquid phase epitaxy (LPE). However, recently, many reports exist of GaSb epitaxy by vapour phase epitaxy (VPE), chemical vapour deposition (CVD), metal-organic chemical vapour deposition (MOCVD), molecular beam epitaxy (MBE) and plasma assisted epitaxy (PAE). But, the technology of GaSb epitaxy is infancy and current research and developments are focussed on areas of high quality materials growth, better understanding of electronic and photonic properties and fabrication of suitable device structures.

J.M. Kang et al [15] investigated the accommodation of lattice mismatch and threading dislocation in MBE grown GaSb on GaAs substrate by the different growth temperature. Their results shown that the lattice mismatch between GaSb and GaAs is relieved mostly by regular 90° misfit dislocations generated during the island growth of GaSb at the 420 ~ 470 °C. At the high temperature (520 °C), 60° dislocations arrays replace some of 90° dislocation, which results in the bending of GaSb film. Even though very regular 90° misfit dislocations can be generated through island growth, the coalescence of islands induces a very high threading dislocation density at a continuous film. In particular, the coalescence at an early stage of growth may result in the threading of 90° misfit dislocations. The spectacular reduction of threading dislocations in large-lattice-mismatched heterostructures will depend on how one can control the random nature of nucleation and coalescence of islands.

H.S. Kim et al [16] used the AlSb buffer layer to grow high quality GaSb film by MBE. They investigated the dependence of micro structural properties of unintentionally doped p-GaSb films grown on thin AlSb islands and rough-and-flat AlSb buffer layers using AFM and HR-TEM. HR-TEM of the thin AlSb islands

buffer layer grown on GaAs substrates revealed 90° misfit dislocations with the Burgers vector of $1/2a \langle 110 \rangle$ at the AlSb/GaAs interface. These defects present the most efficient type of dislocation for the misfit relaxation. By contrast, both 60° and 90° misfit dislocations were observed at the interface between the thick AlSb layer and GaAs substrate. Taken together, their findings for the GaSb layer grown on an AlSb islands confirm that the LT-AlSb islands buffer layer plays a key role in the growth of high-quality GaSb layer.

X.B. Zhang et al [17] reported high quality GaSb was grown on GaAs substrate by using low temperature nucleation GaSb and optimized growth conditions. GaSb with the LT GaSb nucleation layer significantly improves the surface morphology and smoothness. Also, the X-ray results show the improvement of crystallinity by LT nucleation layer as shown figure 1.4. The FWHM is 900 arcsec for GaSb directly grown on GaAs and 288 arcsec for GaSb grown on GaAs with LT GaSb layer, respectively. The much narrow line width indicates that GaSb with LT nucleation GaSb layer is less grainy and the structure quality is significantly improved.

From device point of view, GaSb-based compound semiconductors in devices have been extensively explored because they exhibit the small bandgap and highest mobility of III-V materials. Especially, the optical properties of GaSb have particularly potential for high-speed low-noise avalanche photodetectors (APDs). The ratio of ionization coefficients of holes and electrons k_p/k_n is large [18] and is a key factor in the good APD performance obtained for GaSb.

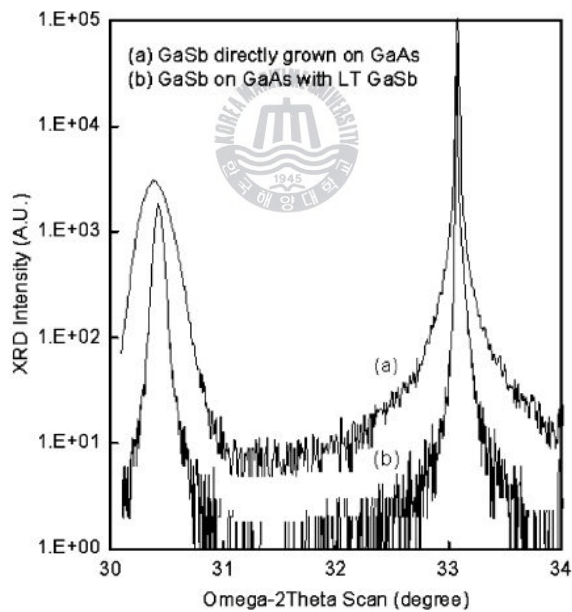


Figure 1.4 (a) and (b) are X-ray ω - 2θ (004) rocking curves of GaSb grown without/with LT-GaSb nucleation layer, respectively

The high ratio of ionization coefficient ($5 \sim 20$) probably exists because of an energy band resonance for the bandgap equal to the spin-orbit splitting, $E_g = \Delta_0$, of the valence band. This condition of high ratio of ionization coefficients particularly applies to $\text{Ga}_{1-x}\text{Al}_x\text{SbAs}$ structure with small x values such as $0.04 \sim 0.06$ [18, 19] and figure 1.5 shows this APDs structure.

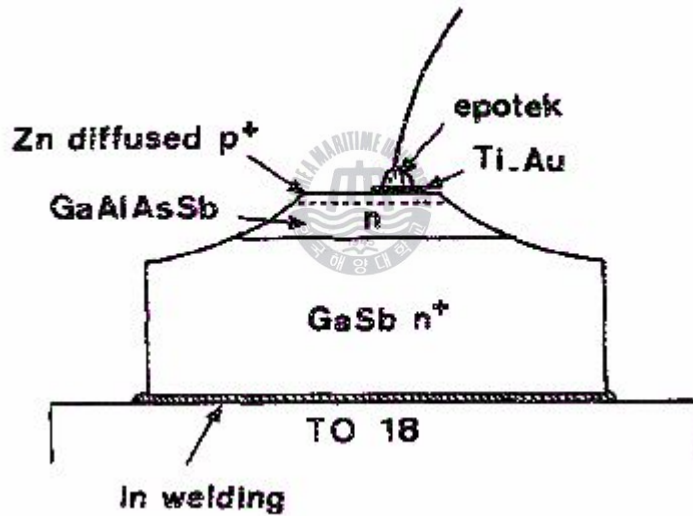


Figure 1.5 Avalanche photodetector structure of GaAlAsSb

The dark current of such diodes tends to be large due to generation in the space charge region and at high reverse voltages there is current produced by tunnelling through deep centers. Growth techniques that minimize the density of deep centers

(natural defects or otherwise) help to reduce the tunnel current to values such as low 10^{-3} A/cm² for reverse voltages in the range 0.5 ~ 0.9 of the breakdown voltage. Avalanche multiplication factors of 30 ~ 50 are obtainable and external quantum efficiencies (without anti-reflection coating) of over 50 % at 1.3 μ m and a sensitivity of 0.6 A/watt. In a study of 1.7 μ m detection a $\text{Al}_{0.053}\text{Ga}_{0.947}\text{Sb}$ *p-n* homojunction avalanche photodiode, figure 1.6 [20] provided a gain of 30 with an excess noise factor (3.8 dB) better than for an APD of GaInAs. LPE grown 10^{17} cm⁻³ n-type $\text{Ga}_{0.82}\text{In}_{0.18}\text{As}_{0.17}\text{Sb}_{0.83}$ layer with Zn diffused *p+* face in the range 1 ~ 1.3 μ m has given rise and fall times of about 50 and 500 ps and the detector responded to pseudomodulation at bit rates up to 2 Gbit/s.



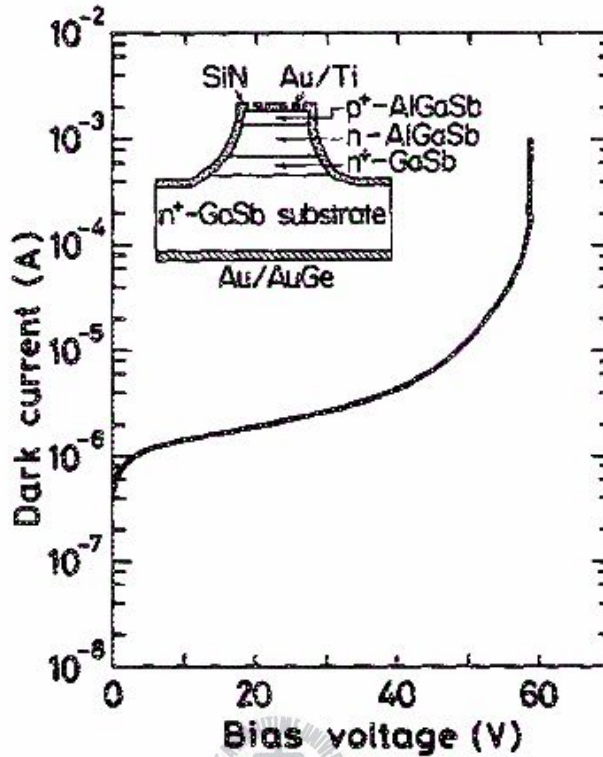


Figure 1.6 Current-voltage characteristic of AlGaSb/GaSb avalanche photodiode.

Inset shows a cross-sectional view of avalanche photodiode.

The high detective has also been reported for $\text{InAs}_{0.85}\text{Sb}_{0.15}/\text{InAs}$ detectors in spite of a 1 % lattice mismatch [21]. Zero-bias detectives D^* of $1.5 \times 10^{11} \text{ cm}(\text{Hz})^{0.5}/\text{W}$ at 77 K and $2 \times 10^{10} \text{ cm}(\text{Hz})^{0.5}/\text{W}$ at 200 K were obtained for a wavelength of 3.5 μm . Such a detector might also be grown on GaSb with less of a

lattice mismatch. Also involved in detector performance are the photo absorption edge of GaSb (300 and 4 K) and these are shown in figure 1.7 [22].

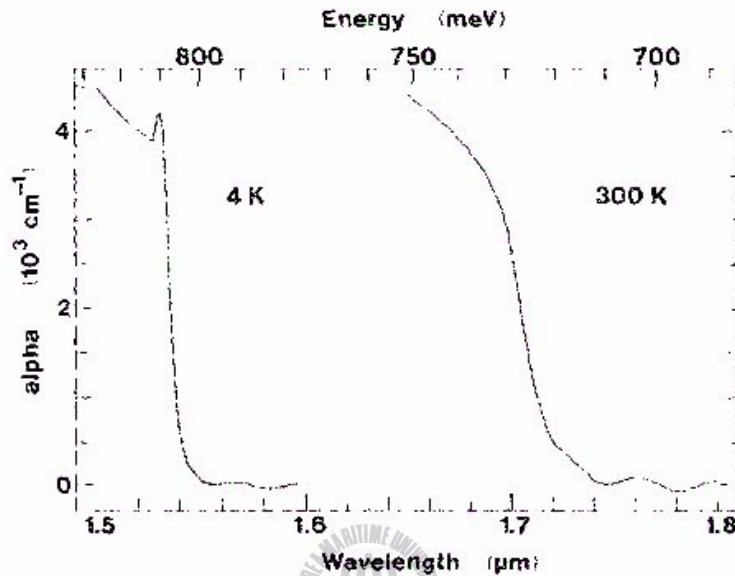


Figure 1.7 Optical absorption spectrum of GaSb at 4 and 300 K.

1.2) Current status of GaSb research

1.2.1) Problems in GaSb heteroepitaxy

GaSb is very useful materials for IR applications, however, the GaSb technology is in its infancy and significant progress has to be made both in materials and processing aspects before it can be employed for device applications. Moreover, most of current researches and developments for the IR optoelectronic

devices used GaSb homoepitaxy to reduce the defects from lattice mismatch. For example, LPE grown alloys of GaAlAsSb and GaInAsSb used on GaSb for APDs [23~25]. Also optical pumping has been used to achieve room temperature laser oscillation at 2.07 μm in a $\text{Ga}_{0.85}\text{In}_{0.15}\text{As}_{0.13}\text{Sb}_{0.87}$ confining layer grown by MBE on GaSb [26].

However, these GaSb homoepitaxy make difficultly the development of GaSb technology for IR application, since high quality GaSb wafer or GaSb substrate is not commercially available yet due to high price and small diameter. In other words, the high quality GaSb growth has been restricted due to the lack of suitable substrate for heteroepitaxy. Because the crystallinity of GaSb ($L_C = 6.095 \text{ \AA}$) epilayer has been mainly affected by the large lattice mismatch to the conventional substrates such as GaAs ($L_C = 5.653 \text{ \AA}$) and InP ($L_C = 5.869 \text{ \AA}$). Among the conventional substrates, InP provides more less lattice mismatch than GaAs, however, difficulties in substrate preparation hinder a wide use. Consequently, GaAs is regarded as a practical solution for GaSb heteroepitaxy. However GaAs also has a large lattice mismatch (+7.8 %) to GaSb, hence a new system must be required to reduce the lattice mismatch for the high quality GaSb growth.

1.2.2) Proposal of thesis

A lot of approaches have been tested to reduce the lattice mismatch between epilayer and substrate in various compound semiconductor growth. Generally, a buffer layer with graded or staircase composition profile is adopted to grow high quality heteroepitaxy [27]. However, cumbersome and time-consuming processes with highly accurate control of growth conditions are required to improve the crystallinity of the heteroepitaxial layer. Therefore, a new buffer system which is able to reduce the large lattice mismatch is inevitably required to obtain high quality GaSb films on GaAs substrate and it must consist of simple methods.

In figure 1.2, I can find several materials such as AlSb ($L_C = 6.135 \text{ \AA}$), InAs ($L_C = 6.058 \text{ \AA}$) and ZnTe ($L_C = 6.103 \text{ \AA}$) which has close lattice constants to GaSb ($L_C = 6.095 \text{ \AA}$). Generally, AlSb buffer layer is used to grow the high quality GaSb due to the small lattice mismatch (0.65 %) [28,29]. However, ZnTe has the smallest lattice mismatch (0.14 %) to GaSb, it is regarded as one of the best buffer layer for the GaSb heteroepitaxy. Therefore, a new buffer layer system which uses the ZnTe should develop to grow high quality GaSb on GaAs.

1.3) Outline of thesis

In this thesis, I suggest to employ ZnTe as a new buffer for the growth of GaSb on GaAs substrate and the growth of the high quality GaSb by using three-step ZnTe buffer layer. Also, we believe that the crystallinity of GaSb is can be improved further through the optimization GaSb/ZnTe heterointerface.

The chapter 2 is an introduction of the principles and used measurement equipments, such as molecular beam epitaxy (MBE), atomic force microscopy (AFM), High resolution X-ray diffraction (HR-XRD), and cathodoluminescence (CL) to investigate the grown GaSb layer. To achieve the high crystallinity of grown GaSb layer, it is important to know its fundamental properties through many analysis systems

In chapter 3, I grow the ZnTe layer by using low-temperature (LT) ZnTe layer to use the buffer layer for high quality GaSb growth and investigate the role of LT-ZnTe buffer layer, because ZnTe also has a large lattice mismatch (+7.9 %) to GaAs substrate. Therefore, ZnTe layer must be optimized to grow high quality GaSb. The lattice deformation of grown ZnTe is greatly reduced by introducing the LT-ZnTe buffer layer.

In chapter 4, we report on the MBE growth of GaSb layer by using three-step ZnTe buffer layer. The effect of three-step ZnTe buffer layer to the surface and structural quality of GaSb layer is investigated. Two-dimensional reciprocal space mapping (RSM) results of the GaSb layers clearly indicate that the structural deformation of the GaSb layer is greatly reduced by introducing the ZnTe buffer, which makes remarkable improvement of the crystallinity of GaSb layer.

In chapter 5, GaSb films are grown on two distinct surfaces of ZnTe layers and the influence of surface chemical composition of ZnTe on the structural properties and luminescence of GaSb film is investigated. Initial 2-dimensional growth of GaSb films occurs on Zn-terminated surface consequently smooth morphology and high crystal quality GaSb films are achieved. Also cathodoluminescence results show that considerable feature originated from the GaSb/ZnTe has not been observed presumably due to high interface quality, which strongly supports the availability of ZnTe buffer for high quality GaSb growth.

In chapter 6, I describe the summary and conclusion of this thesis.

Reference

- [1] R.C. Sharma, T. Leo and Y.A. Chang, *J. Electron. Mater.* 16, 307 (1987)
- [2] A.G. Milnes and A.Y. Polyakov, *Solid-state Elec.* 36, 803 (1993)
- [3] R.D. Baxter, R.T. Bate and F.J. Reid, *J. Phys. Chem. Solids* 26, 41 (1965)
- [4] K. Nakashima, *J. J. appl. Phys.* 20, 1085 (1981)
- [5] K.F. Longenbach and W.I. Wang, *Appl. Phys. Lett.* 59, 2427 (1991)
- [6] H. Xie, J. Piao, J. Katz and W.I. Wang, *J. Appl. Phys.* 70, 3152 (1991)
- [7] G. Motosugi and T. Kagawa, *J. J. Appl. Phys.* 19, 2303 (1980)
- [8] M.B.Z. Morosini, J.L. Herera-Perez, M.S.S. Loral, A.A.G. Vonzuben, A.C.F. da Silveira, and N.B. Patel, *IEEE J. Quantum Electron.* QE-29, 2103 (1993)
- [9] Q. Hildebrand, W. Kuebart, K.W. Benz, and M.H. Pilkuhn, *IEEE J. Quantum Electron* QE-17, 284 (1981)
- [10] K. Segawa, H. Miki, M. Otsubo, and K. Shirata, *Electron. Lett.* 12, 124 (1976)
- [11] C. Hilsum and H.D. Rees, *Electron. Lett.* 6, 277 (1970)
- [12] L. Esaki, *J. Cryst. Growth* 52, 227 (1981)
- [13] P.S. Dutta, H.L. Bhat, Vikram Kumar, *J. Appl. Phys.* 81, 5821 (1997)
- [14] H. Xie, J. Piao, J. Katz and W.I. Wang, *J. Appl. Phys.* 19, 2303 (1980)

- [15] J.M. Kang, M. Nouaoura, L. Lassabatere, A. Rocher, J. Cryt. Growth 143, 115 (1994)
- [16] H.S. Kim, Y.K. Noh, M.D. Kim, Y.J. Kwon, J.E. Oh, Y.H. Kim, J. Y. Lee, S.G. Kim, K.S. Chung, J. Crys. Growth 301-302, 230 (2007)
- [17] X.B. Zhang, J.H. Ryou, R.D. Dupuis, S. Mou, S.L. Chuang, C. Xu, K.H. Hsieh, J. Crys. Growth 287, 545 (2006)
- [18] H. Luquet, M.perotin, L. Gousskov, C. Llinares, H. Archidi, M. Lahbadi, M. Karim and B. Mbow, J. Appl. Phys. 68, 3861 (1990)
- [19] M. M. Mebarki, T. Belatoui, A. Joullie, B. Orsal and R. Alabedra, J. Appl. Phys. 68, 4106 (1990)
- [20] S. Miura, T. Mikawa, H. Kuwatsuka, N. yasuoka, T. Tanahashi and O. Wada, Appl. Phys. Lett. 54, 2422 (1989)
- [21] K. Mohammed, F. Capasso, R.A. Logan, J.P. van der Ziel and A.L. Hutchinson, Electron. Lett. 22, 215 (1986)
- [22] A.M. Fox, A.C. Maciel, J.F. Ryan and T. Kerr, Appl. Phys. Lett. 51, 430 (1987)
- [23] Y. Takeda, S. Noda and A. Sasaki, J. Appl. Phys. 57, 1261 (1985)

- [24] S.C. Chen, Y. K. Su and F.S. Juang, *J. Cryst. Growth* 92, 118 (1988)
- [25] M. Ichimura, K. Higuchi, Y. Hattori, T. Wada and N. Kitamura, *J. Appl. Phys.* 68, 6153 (1990)
- [26] J.P. van der Ziel, T.H. Chiu and W.T. Tsang, *J. Appl. Phys.* 60, 4087 (1986)
- [27] H. Amano, N. Sawaki, I. Akasaki and Y. Toyoda, *Appl. Phys. Lett.* 48, 353 (1996)
- [28] H. Toyota, T. Sasaki, Y. Jinbo and N. Uchitomi, *J. Cryst. Growth* 310, 98 (2008)
- [29] K. Akahane, N. Yamamoto, S. Gozu and N. Ohtani, *J. Cryst. Growth* 264, 21 (2004)



Chapter 2. Experiment

2.1) Epitaxy

Epitaxy is a composed word by “epi” + ”taxy”, where “epi” means “on” or “above” and “taxy” means “order” or “arrange”. Therefore, epitaxial growth means a technique to deposit a material on a substrate with single orientation. Consequently, the substrate acts as a seed crystal, the deposited material takes on a lattice structure and orientation identical to those of the substrate.

As shown figure 2.1, epitaxy is classified two parts by relationship between epitaxial layer and substrate and it is homoepitaxy and heteroepitaxy, respectively.

Homoepitaxy is a kind of epitaxy performed with only same material. In homoepitaxy, a crystalline layer is grown on a substrate or epitaxial layer of the same material. Heteroepitaxy is a kind of epitaxy performed with materials that are different from each other. In heteroepitaxy, a crystalline layer grows on a crystalline substrate or layer of another material.

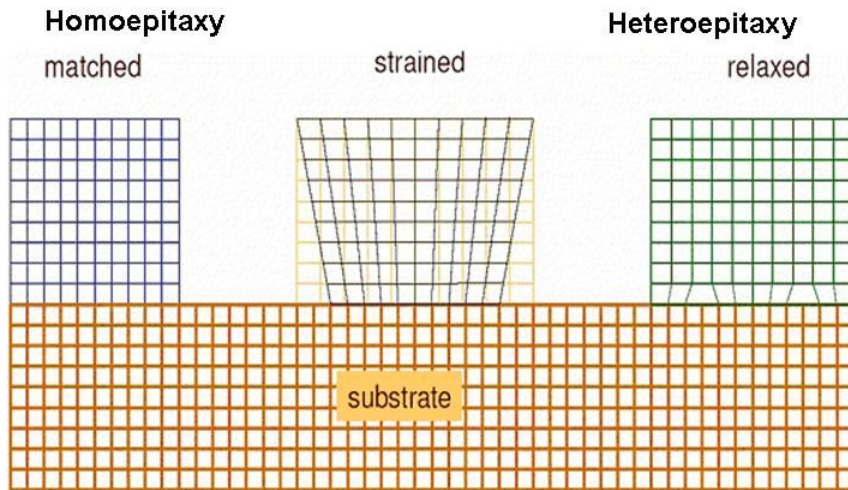


Figure 2.1 Classification of epitaxy

2.2) Three-types of epitaxial growth

Epitaxial growth is generally accepted that three possible modes of crystal growth on surfaces may be distinguished. These modes are illustrated schematically in figure 2.2. In case of island (Volmer-Webber growth mode) growth, small clusters are nucleated. This happens when the physisorbed atoms are more strongly bound to each other than substrate [1].

The layer-by-layer (Frank-van der Merwe mode) growth displays the opposite characteristics because the atoms are more strongly bound to the substrate than to each other. The first atoms to condense form a complete monolayer on the surface,

which becomes covered with a somewhat less tightly bound second layer. Provided the decrease in binding is monotonic toward the value for a bulk crystal of the deposit, the layer growth mode is obtained [1].

The layer plus island (Stranski-Krastanov mode) growth is an intermediate case. After forming the first monolayer, or a few monolayers, subsequent layer growth is unfavorable and islands are formed on top of this “intermediate” layer. There are many possible reasons for this mode to occur and almost any factor which disturbs the monotonic decrease in binding energy characteristic for layer-by-layer growth may be the cause [2].

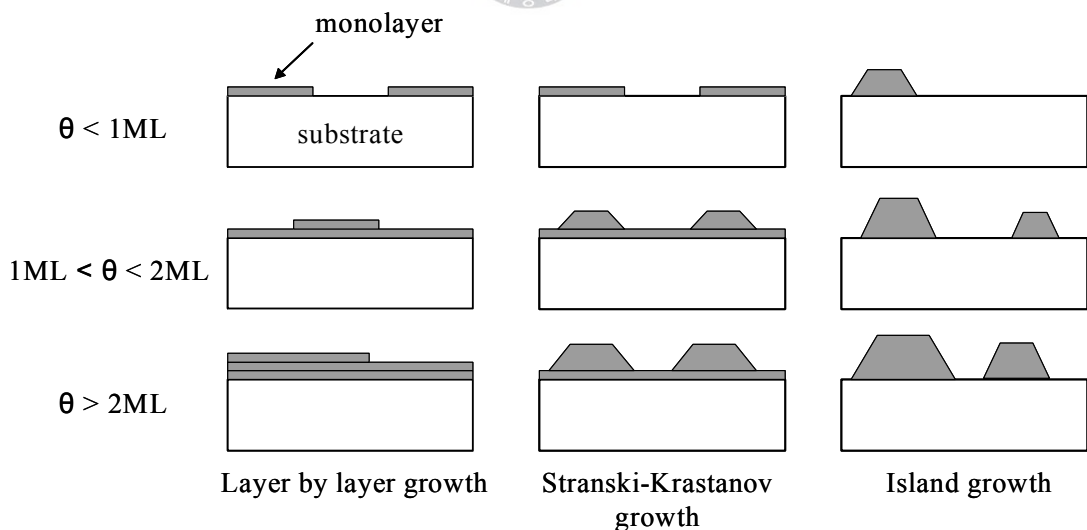


Figure 2.2 Schematic representation of the three crystal growth modes. θ represents the coverage in monolayer.

2.3) Molecular Beam Epitaxy

Molecular beam epitaxy (MBE) is a versatile technique for growing epitaxial structures made of semiconductors, metals or insulators. In MBE, epitaxial layers crystallize via reactions between thermal-energy molecular or atomic beams of the constituent elements and a substrate surface which is maintained at an elevated temperature in ultra high vacuum. The growth rate is low enough that surface migration length of the impinging species on the growing surface is ensured. Consequently, the surface of the grown layer is very smooth.

Figure 2.3 shows the surface processes occurring during MBE growth. The substrate crystal surface is divided into so-called crystal sites where the impinging atoms may interact. Each crystal site is a small part of the crystal surface characterized by its chemical activity. A site may be created by a dangling bond, vacancy, step edge and etc.

In comparison to all other epitaxial growth techniques, MBE has a unique advantage. Being realized in an ultrahigh vacuum environment, it may be controlled in situ by surface sensitive diagnostic method including reflection high energy electron diffraction (RHEED). This powerful facility for control and

analysis eliminates much of the guesswork in MBE, and enables the fabrication of sophisticated device structures using this growth technique.

MBE is composed of vacuum system (vacuum pumps), source supply system (k-cell, cracking-cell, plasma etc.), substrate handling system (transfer-rod, substrate holder, carrier etc.), and in situ surface diagnosis (RHEED observation system). Figure 2.3 shows the MBE system. Background vacuum is a very important factor to obtain high purity epitaxial layers, since the residual gas in vacuum system would act as impurities. Generally, the background pressure in the range of low 10^{-10} torr to mid 10^{-11} torr is used to grow a sufficiently pure epilayer and to obtain the enough sticking coefficients of constituent atoms.

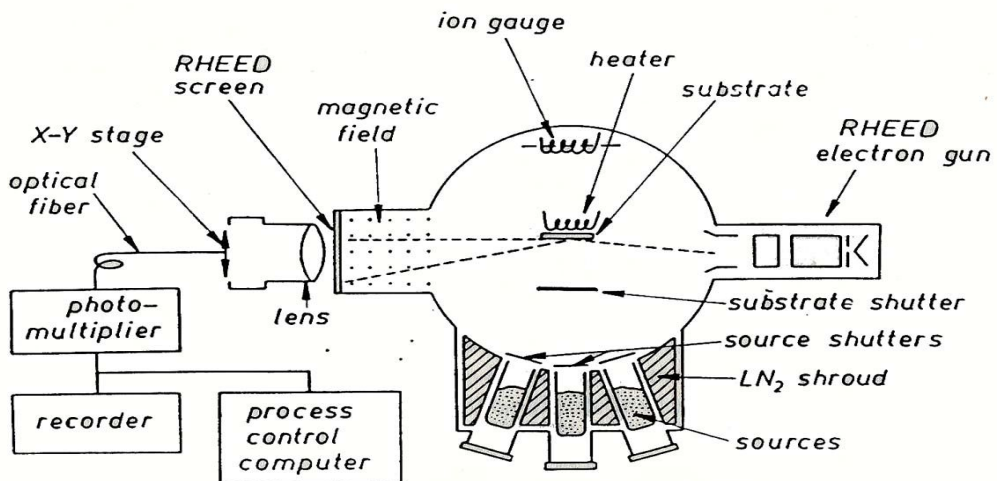


Figure 2.3 Schematic illustration of molecular beam epitaxy system

For the source supply system, conventional Knudsen-cells (Zn, Se, Te, Ga, Sb) are used. The effusion cells (K-cell) have an operating temperature range of up to 1400 °C, depending on the purpose of the sources such as growing or doping, the size and shape of crucibles are different. The source material determines the temperature range of the K-cells. Simple mechanical shutters in front of K-cells are used to control the beam fluxes for growth. Those features distinguish MBE from the conventional vacuum deposition techniques.

A substrate is mounted on a substrate holder by using In. The substrate holder is heated for cleaning of substrate and for growing on the substrate. Out gassing from a substrate holder and a heater during heating should be minimized. The selection of materials of the substrate holder and heater is crucial for reducing out-gas.

2.4) Reflection high energy electron diffraction: RHEED

Reflection high energy electron diffraction (RHEED) is used to analysis various information during epitaxial growth in ultra high vacuum (UHV)-chamber. In conditions which are usually employed in MBE a high energy beam of electrons in the range of 5 ~ 30 keV is incident at low angle ($1 \sim 3^\circ$) to the surface. The

RHEED pattern generated by the sample surface was displayed on a phosphor screen located at the opposite side of the RHEED gun and was captured using a CCD camera controlled by computer as shown in figure 2.4.

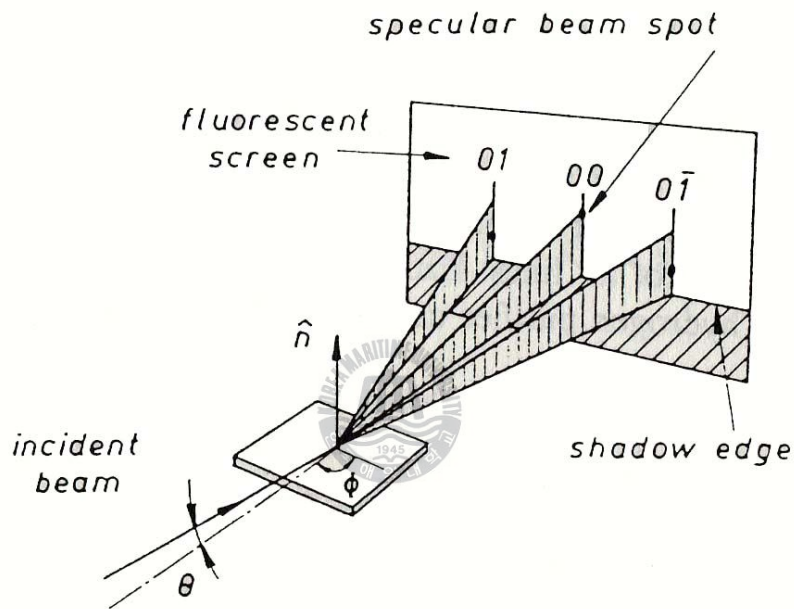


Figure 2.4 Schematic illustration of RHEED observation

The de Broglie wavelength of these electrons is in the range of $0.06 \sim 0.17 \text{ \AA}$ and the penetration of the beam into the surface is low, being restricted to the

outermost few atomic layers [3]. Generally, the wavelength λ corresponding to an accelerating voltage V is given to a good approximation by

$$\lambda \approx \frac{12.247}{\sqrt{V + 10^{-6}V}} \text{ [\AA]} \quad (2.1)$$

Most geometrical aspects of the diffraction pattern can be interpreted on the basis of a limited penetration scattering model, i.e., a model which is kinetic in the diffraction sense [4]. The detailed analysis of the diffracted beam intensity particularly the way in which it changes with incident angle (θ in figure 2.4) should in principle permit an exact determination of the complete structure of the surface unit cell.



When the electron beam is incident on a plane with mirror index (hkl) , the electron beam is elastically scattered at the (hkl) plane. The condition for diffraction is given by the Bragg condition:

$$2d_{hkl}\sin\theta = n\lambda \quad (n = 1, 2, \dots) \quad (2.2)$$

Where d_{hkl} is the interplanar distance of the plane (hkl) , θ is the angle between the incident electron beam and the plane, and λ is the electron wavelength.

The diffraction process in RHEED is not always ideal reflection, which will produce two different patterns on the RHEED screen. In the first case the

diffraction pattern exhibits spotty features, while in the second case, the RHEED pattern shows streaks, if the surface has a roughness of atomic layer thickness.

Using the Bragg equation and the Ewald sphere construction, one may deduce the periodicity of the surface atomic structure by measuring the distance between diffraction spots or rods. The in-plane lattice constant d can be calculated using the relation:

$$d = 2\lambda L/D \quad (2.3)$$

where λ is the electron wavelength, L is the distance between the sample and the screen, and D is the distance between the adjacent reciprocal rods on the screen.

This equation can be applied to the calculation of surface lattice constant during growth. It is possible to investigate the growth dynamics of MBE by monitoring temporal variation of the intensity of various spots in RHEED pattern. Oscillations of the specular spot intensity and the diffraction spot intensity are observed during two-dimensional MBE growth. The period of oscillation corresponds exactly to the growth of single monolayer. In figure 2.5, a real space representation of the formation of the first two complete layers is shown. This illustrates how the oscillation of the specular spot intensity occurs. There is a maximum in intensity

for the initial and final smooth surfaces and a minimum in intensity (or maximum intensity in diffuse scattering) for the intermediate stage, where the grown layer is approximately half complete. And the maximum diffuse scattering is caused when their longer edges are normal to the incident beam. Therefore, it may conclude that the growth occurs principally by a two-dimensional layer-by-layer process, but new layers are able to be started before preceding ones have been completed.

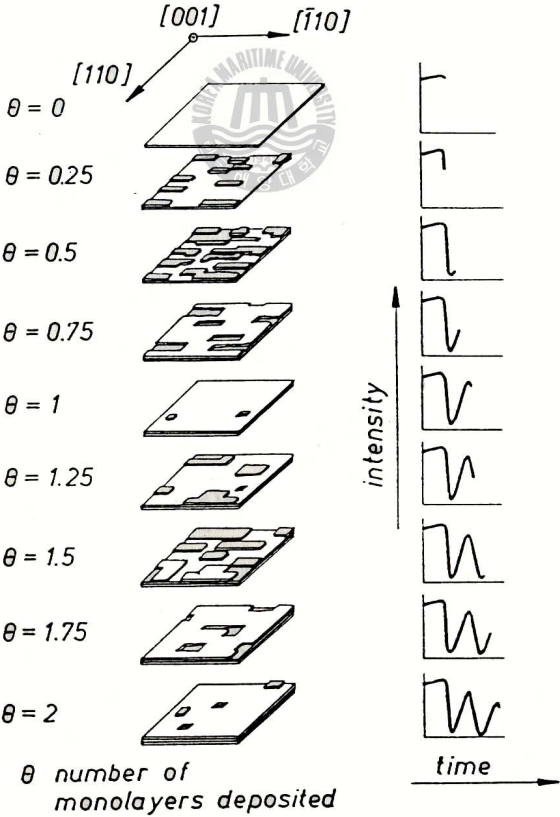


Figure 2.5 RHEED specular spot intensity

The oscillation period provides continuous and absolute growth rate monitor with atomic layer precision. Therefore, these properties by using RHEED pattern observation and RHEED intensity oscillation are very useful methods to establish the dynamic growth and to determine the growth condition.

2.5) Atomic Force Microscopy (AFM)

The AFM consists of a microscale cantilever with a sharp tip (probe) at its end that is used to scan the specimen surface. The cantilever is typically silicon or silicon nitride with a tip radius of curvature on the order of nanometers. When the tip is brought into proximity of a sample surface, forces between the tip and the sample lead to a deflection of the cantilever according to Hooke's law. Depending on the situation, forces that are measured in AFM include mechanical contact force, Van der Waals forces, capillary forces, chemical bonding, electrostatic forces, magnetic forces, Casimir forces, solvation forces etc. As well as force, additional quantities may simultaneously be measured through the use of specialized types of probe. Typically, the deflection is measured using a laser spot reflected from the top of the cantilever into an array of photodiodes. Other methods that are used

include optical interferometry, capacitive sensing or piezoresistive AFM cantilevers. These cantilevers are fabricated with piezoresistive elements that act as a strain gauge. Using a Wheatstone bridge, strain in the AFM cantilever due to deflection can be measured, but this method is not as sensitive as laser deflection or interferometry.

If the tip were scanned at a constant height, there would be a risk that the tip would collide with the surface, causing damage. Hence, in most cases a feedback mechanism is employed to adjust the tip-to-sample distance to maintain a constant force between the tip and the sample. Traditionally, the sample is mounted on a piezoelectric tube that can move the sample in the z direction for maintaining a constant force, and the x and y directions for scanning the sample. Alternatively a 'tripod' configuration of three piezo crystals may be employed, with each responsible for scanning in the x, y and z directions. This eliminates some of the distortion effects seen with a tube scanner. The resulting map of the area $s = f(x, y)$ represents the topography of the sample. Fig 2.6 shows the schematic illustration of AFM.

The AFM can be operated in a number of modes, depending on the application.

In general, possible imaging modes are divided into static (also called contact) modes and a variety of dynamic (or non-contact) modes.

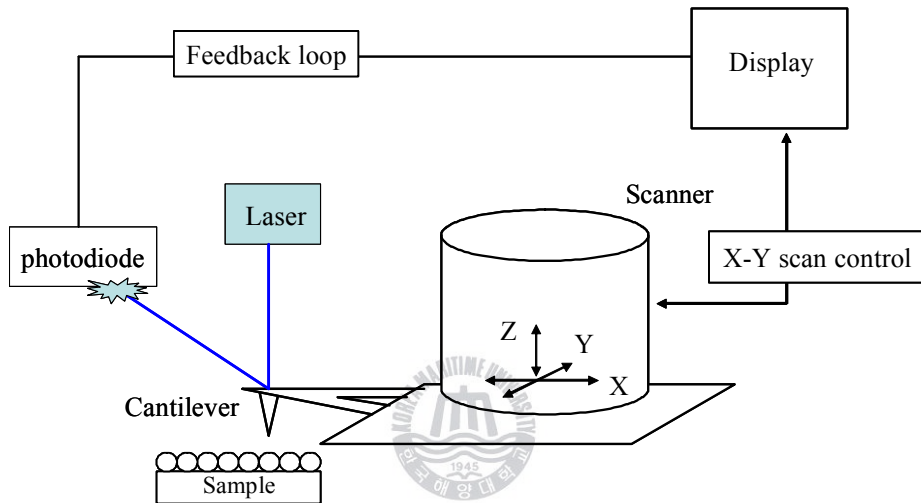


Figure 2.6 Schematic illustration of AFM

2.6) High resolution X-ray diffraction (HR-XRD)

2.6.1) Conventional high resolution X-ray

Conventional high resolution X-ray diffraction (HR-XRD) is a powerful tool for the non-destructive ex-situ investigation of epitaxial layers. The information

which is obtained from diffraction patterns concerns the composition and uniformity of epitaxial layers, their thicknesses, the built-in strain and strain relaxation, and the crystalline perfection related to their dislocation density [5].

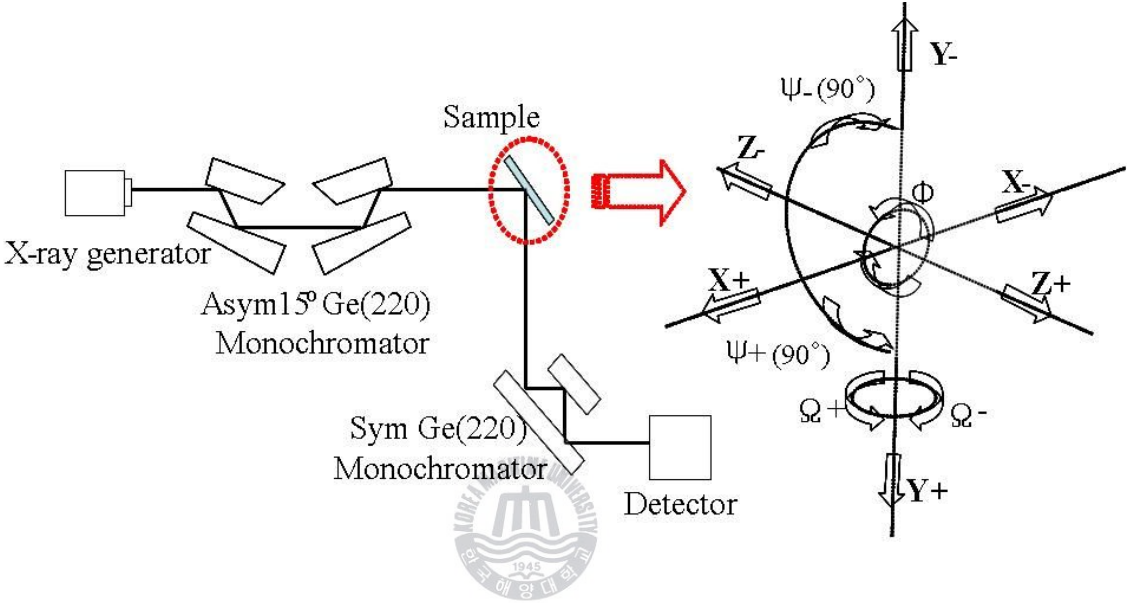


Figure 2.7 Schematic illustration of HRXRD geometry

Figure 2.7 shows the schematics of X-ray measurement system. It combines a four-crystal monochromator and a multiple-reflection analyzer crystal to perform high-resolution measurements for reciprocal lattice scans. The Ge (220) 4-crystal monochromator added by the crossed slit attachment is used as an X-ray beam source. The Ge 4-crystal monochromator produces a beam with very low

divergence and small wavelength spread. For example, approximate divergence of the Ge (220) 4-crystal monochromator is 12 arcsec. The crossed slit collimator is designed to provide a point x-ray source. The slit is variable in width up to 10 nm with a step of 0.02 mm. The diffracted beam is detected by a double arm attachment which is used for high resolution application. One arm is a rocking curve attachment and the second arm carries the channel cut analyzer crystal to convert to a triple axis mode. A Ge crystal with symmetric (220) reflection was used for the analyzer. For the X-ray scans, a beam of parallel and monochromatic x-rays of wavelength λ is incident on a crystal at an angle θ_B , Bragg angle, which is measured between the direction of the incident beam and the crystal plane under consideration.

2.6.2) ω scan (rocking curve) and ω -2 θ scan

Any measurement of lattice spacing is in principle determined by Bragg law (equation 2.2). This equation follows from kinematic diffraction theory and neglects the fact that the refractive index of matter for X-ray is less than 1 by a

few parts in 10^{-6} and so the incident beam is refracted to an internal angle slightly smaller than the external one.

In figure 2.8, two possible scans for measuring the intensity of Bragg reflection due to the reciprocal lattice point (hkl) are indicated:

(i) Conventional powder diffraction uses a ω - 2θ scan for measuring symmetric Bragg reflections. For such a scan, the detector is rotated twice as fast and in the same direction around the diffractometer axis as the sample. In reciprocal space (Figure 2.9), this conventional motion of sample and detector corresponds to a change of k_s in the following way: the tip of vector k_s moves along the reciprocal lattice vector G_{hkl} . During this motion the angle ω between the incident beam and the sample surface changes. For asymmetric (hkl) Bragg reflections, ω - 2θ scan direction runs also radial from the origin (000) of the reciprocal space along G_{hkl} (Figure 2.8a)

(ii) In the ω -scan, the detector is fixed in position with wide open entrance slits and the sample is rotated, i.e. ω changes. In reciprocal space, this corresponds to a path as indicated in figure 2.8b by bold arrow. The scan direction is transversal in

reciprocal space. Thus the so-called rocking curve is obtained. In reciprocal space, this corresponds to a path as shown in figure 2.9

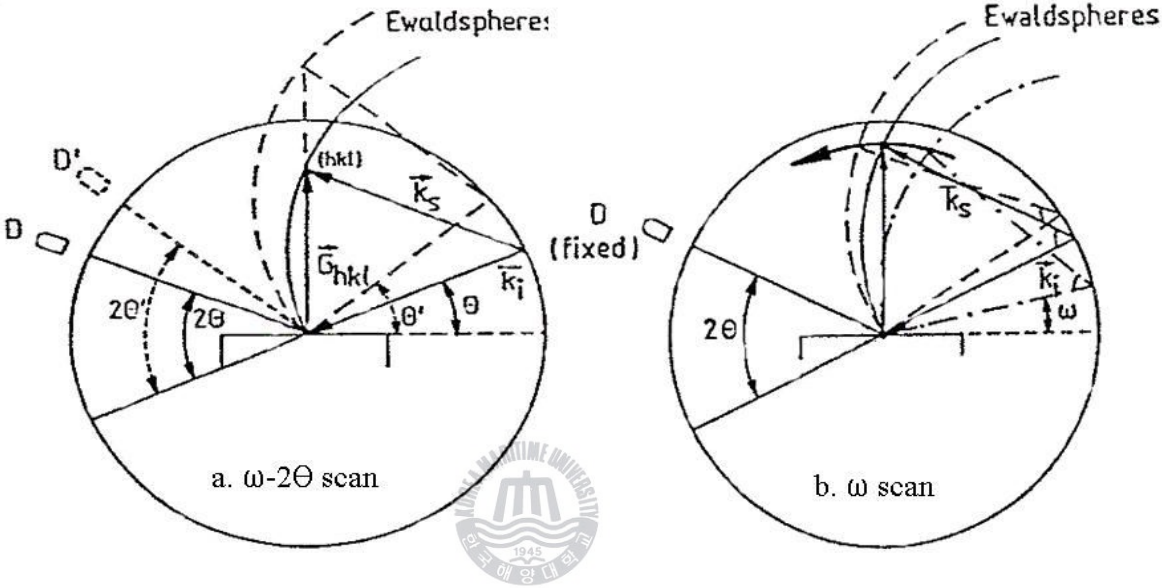


Figure 2.8 Ewald sphere construction (for symmetric reflections, i.e. reflecting planes are parallel to the surface) for the ω - 2θ scan geometry. The bold arrow indicates the movement in the reciprocal lattice

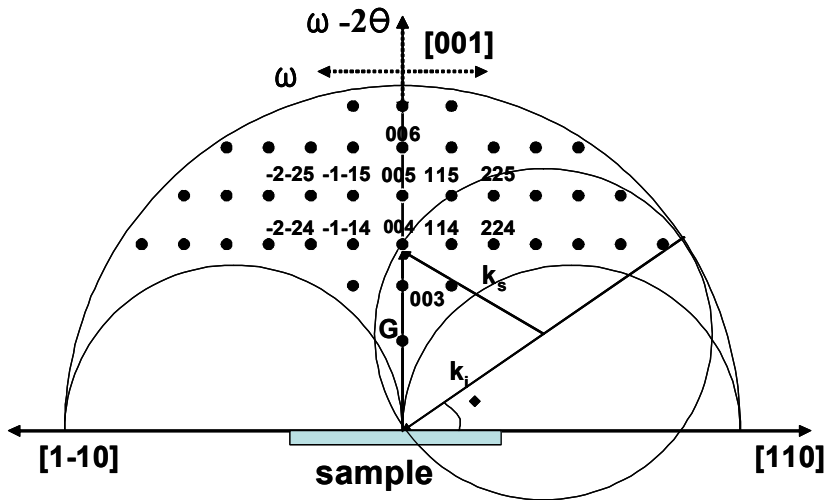


Figure 2.9 Reciprocal space map showing accessible range for Bragg reflection

measurement.



When we consider about rocking curve of heteroepilayers, there exist difference of diffraction angle between the layer and substrate, which is caused by tilt or mismatch. Double or multiple peaks will therefore arise in the rocking curve. Peaks may be broadened by defects if these give additional rotations to the crystal lattice, and there will also be small peaks arising from interference between waves scattered from the interfaces, which will be controlled by the layer thickness. The

material will show different defects in different regions. Table 2.1 summarizes the influence on the rocking curve of the important parameter [6].

Table 2.1. The effects of substrate and epilayer parameters upon the rocking curve.

Material parameter	Effect on rocking curve	Distinguishing features
Mismatch	Splitting of layer and substrate peak	Invariant with sample rotation
Misorientation	Splitting of layer and substrate peak	Changes sign with sample rotation
Dislocation content	Broadening peak	Broadening invariant with beam size No shift of peak with beam position on sample.
Mosaic spread	Broadening peak	Broadening may increase with beam size, up to mosaic cell size
Curvature	Broadening peak	Broadening increases linearly with beam size Peak shifts systematically with beam position on sample
Relaxation	Changes splitting	Different effect on symmetrical and asymmetrical reflection

Thickness	Affects intensity of Peak	Integrated intensity increases with layer thickness, up to a limit
Inhomogeneity	Effects vary with position on sample	Individual characteristics may be mapped

2.7) Cathodoluminescence (CL)

Cathodoluminescence (CL) is the emission of light under an electron bombardment. Cathodoluminescence can provide contactless and nondestructive and depth-/spatial- analysis of a wide range of electronic properties of a variety of luminescent materials. The excitation depth can be varied from about 10 nm to several μm for electron-beam energies. And it is an optical and electrical phenomenon where a beam of electrons generated by an electron gun (e.g. cathode ray tube) impacts on a phosphor causing it to emit light. In geology, a CL is used to examine internal structures of rock samples in order to study the history of the rock.

The incident electrons in CL system are absorbed by the material and generate electron-hole pairs that may lead to the emission of photons, what is called radiative de-excitation. Indeed, as shown in figure 2.10, the pairs diffuse in the material and recombine each other. This recombination may produce photons

whose energy depends on the energy level of the center where the electron and the hole are captured. This center is called the recombination center. However, the deexcitation may also be due to phonons that are emitted by surface states, defects, Auger process... This phenomenon is the nonradiative deexcitation.

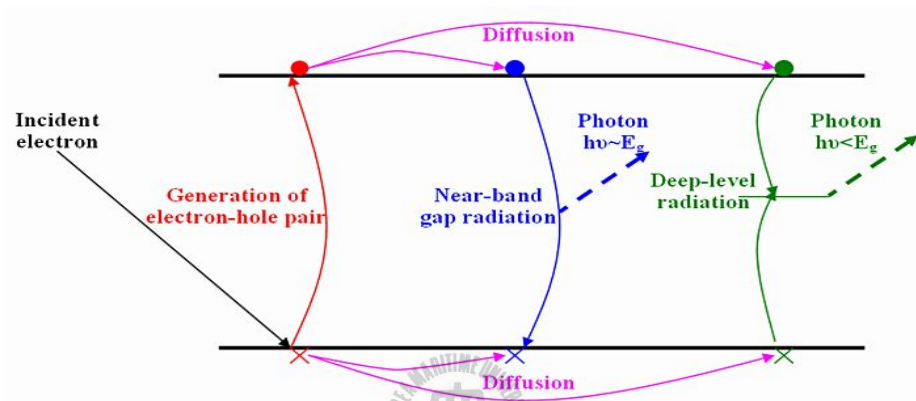


Figure 2.10 Diagram of generation and recombination of electron-hole pairs

The incident electron beam interacts with the material. It undergoes a successive series of elastic and inelastic scattering events that randomize the trajectories of the incident electrons. The deviation may be large compared to the original trajectory. The scattered electrons form contours in the form of “mushrooms”. As shown in figure 2.11, the visualization of the volume of

interaction between the electron beam and the material may be done by the Monte Carlo method [7].

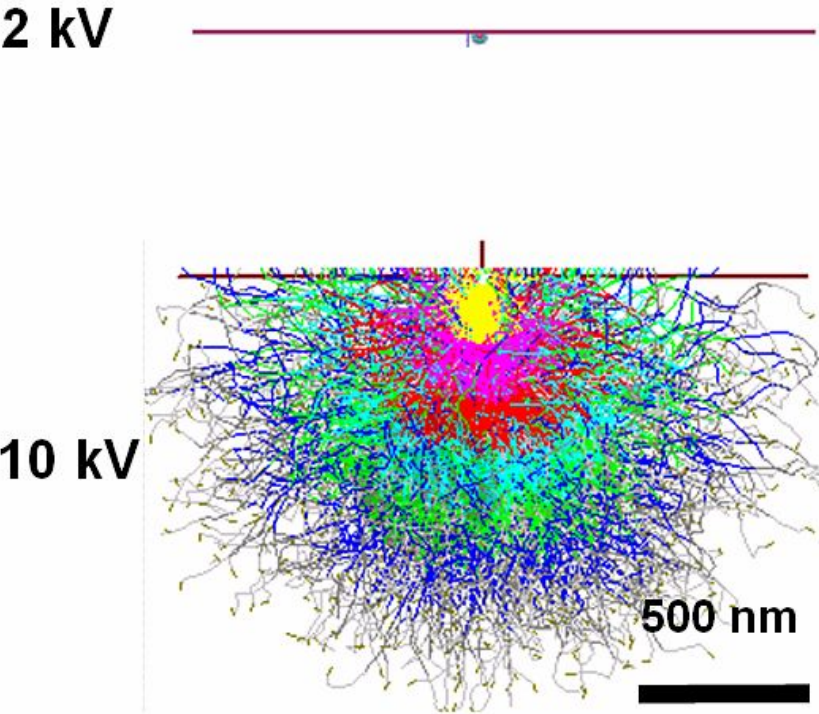


Figure 2.11 Simulation of the scattered electrons by the Monte Carlo method

Moreover, as it may be seen in figure 2.12 the range of the electron penetration is a function of the accelerating voltage V_b : the electron range R_e is proportional to

$V_b^{1.75}$, the linear coefficient depending on the material characteristics. So, the increasing of the accelerating voltage allows us to characterize deeper areas and so the influence of the depth-resolved luminescence

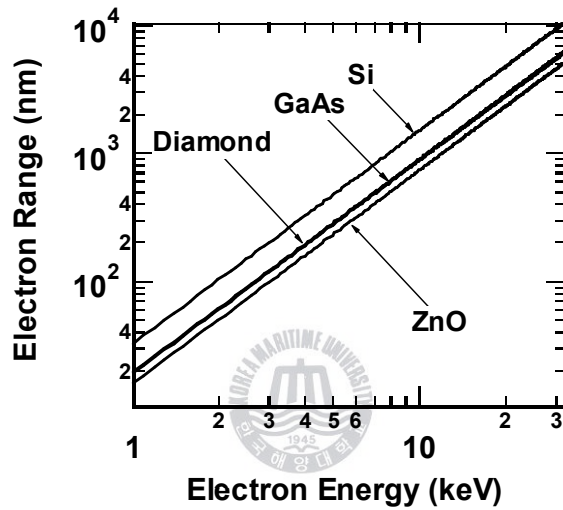


Figure 2.12 Correspondence between the electron range and the electron penetration

The excitation of cathodoluminescence is very important: 1 E-keV incident electron may generate, in a material whose energy gap is E_g , $E/3E_g$ electron-hole pairs. Moreover, contrary to the photoluminescence where selective excitations

cause particular emission processes, electron beam excitation may activate all luminescence mechanisms present in the material. On the other hand, the generation rate of electron-hole pairs g is proportional to the accelerating voltage V_b and the beam current I_b . Consequently, the generation density $d_{\text{generation}}$ within the irradiated volume is:

$$d_{\text{generation}} = g / \text{volume} = \frac{g}{4/3 R_e^3} \quad (2.4)$$

$$d_{\text{generation}} \approx \frac{V_b * I_b}{(V_b^{1.75})^3} \quad (2.5)$$

$$d_{\text{generation}} \approx V_b^{-4.25} * I_b \quad (2.6)$$

So, the generation density increases with increasing the beam current and decreases quickly with increasing accelerating voltage [8].

Reference

- [1] M.A. Hreman, h. Sitter, Molecular Beam Epitaxy, 1st edition (Springer-Verlag Berlin heidelberg, 1998), p12
- [2] J.A. Venables, G.D.T. Spiller, M. Hanbuecken, Rep. Prog. Phys. 47, 399 (1984)
- [3] P.J. Dobson, B.A. Joyce, J.H. Neave, J. Zhang, J. Cryst. Growth 81, 1 (1987)
- [4] E. Bauer: "Reflection Electron Diffraction", in Techniques of Metals Research Vol. 2, ed. by R.F. Bunshah (Wiley-Inter science, New York 1969) Chap. 15
- [5] Günther Bauer, Wolfgang Richter, "Optical Characterization of Epitaxial Semiconductor Layers" 1st edition (Springer-Verlag Berlin heidelberg, 1996), p287
- [6] D.K. Bowen and B.K. Tanner: "High resolution X-ray Diffraction and Topography" (Taylor & Francis Ltd, London, United Kingdom, 1998), p52
- [7] B.G. Yacobi and D.B. Holt: "Cathodoluminescence microscopy of inorganic solids" (plenum pres, New York, 1990), p63
- [8] H.J. Leamy, J. Appl. Phys. 53, R51 (1982)

Chapter 3. Structural deformation reduction of MBE grown ZnTe by LT-buffer

3.1) Introduction

Heteroepitaxy provides a wide range of freedom for the different kinds of material growth of mismatched systems. However, for the growth of high quality heteroepitaxial layers, one should solve the problem of accommodation of the various mismatches between substrates and epitaxial layers. Buffer layer growth is a widely adopted technique not only for heteroepitaxy, but also for homoepitaxy to accommodate mismatches and to grow high quality film. It is understood that the buffer layer performs four important roles such as (1) heterointerface formation, it is especially important for the heteroepitaxy with heterovalency, (2) accommodation of lattice mismatch, actually it is the main role of a buffer, (3) dislocation reduction, it is obtained through the various ways such as bending, interaction, and looping of dislocations during the buffer layer growth, and (4) provides optimum surface for epitaxy, a smooth surface enhances two dimensional growth, which is indispensable for the high quality epitaxy [1].

There have been many reports on the role of various buffer layers [2 ~ 4]. Kanisawa et al. [5] reported the reduction of interface fluctuation by using low-temperature buffer for InSb growth. Song et al. inserted a thin ZnSe buffer at low-temperature to reduce stacking faults due to Ga-Se reaction at the heterointerface [6]. Chang et al. reported that low-temperature buffer growth reduces the propagation of dislocation [1].

Since ZnTe has large lattice mismatch (+7.9 %) to GaAs, the high quality ZnTe growth on GaAs has been restricted. Therefore, in this chapter, to grow the high quality ZnTe on GaAs substrate the low-temperature ZnTe buffer (LT-buffer) used and it annealed. The role of LT-ZnTe buffer in terms of the structural quality of the overgrown layer has been discussed by using various methods such as RHEED, XRD and reciprocal space mapping (RSM) results.

3.2) Experimental details

Two samples were prepared for the discussion: sample-A (HT-ZnTe/GaAs) and sample-B (HT-ZnTe/LT-ZnTe/GaAs). The growth procedure was almost similar to the previous report [1] except that ZnSe buffer layer was not grown in this

chapter, because I just intended to observe the effect of LT-ZnTe buffer. GaAs (001) substrates were degreased and etched by using NH_4OH solution. Then it was mounted on Mo-holder using In. Thermal treatment was performed at $640\text{ }^\circ\text{C}$ for 15 min in the ultra-high-vacuum (UHV) chamber to remove the oxide layer on surface. During the thermal treatment of GaAs substrate, (4×2) reconstruction pattern was observed. Its reflection high energy electron diffraction (RHEED) pattern was almost streaky at the end of thermal treatment and it becomes completely streaky when the growth starts. The growth rate was $\sim 300\text{ nm/h}$ and VI/II ratio was controlled to ~ 2 for both samples. LT-ZnTe buffer was grown at $250\text{ }^\circ\text{C}$, and HT-ZnTe buffer layer was grown at $300\text{ }^\circ\text{C}$. High resolution X-ray diffraction measurement (HR-XRD) was used to evaluate the structural quality of the samples, and atomic force microscopy (AFM) was used to observe the surface morphology. Reciprocal space mapping (RSM) was used to investigate the structural deformation of the ZnTe layers.

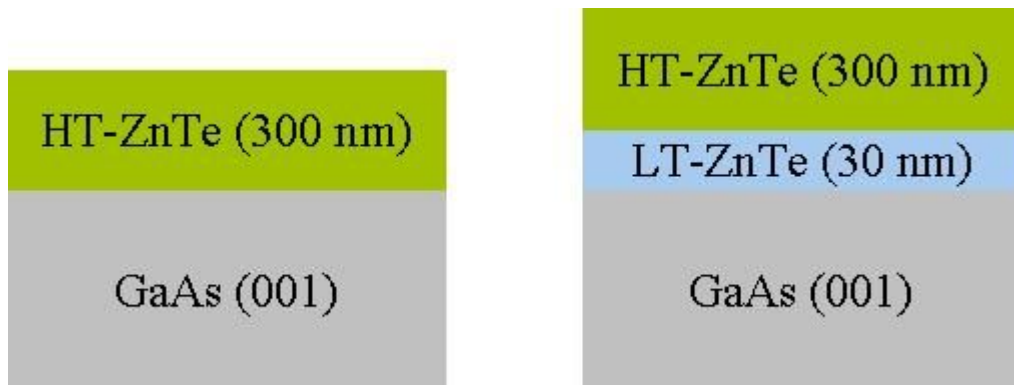


Figure 3.1 Schematic drawing of prepared samples

3.3) Initial growth observation

ZnTe heteroepitaxial layers were grown on GaAs (001) substrates. After finishing the thermal cleaning of the GaAs substrates, the substrate temperature was lowered down to 250 °C to grow LT-ZnTe buffer layer. The thickness of LT-ZnTe buffer was controlled to 30 nm, which is well above the critical thickness of ZnTe [7]. It should be pointed that the critical thickness is a function of growth temperature and interface state [8]. Therefore, even in films having same thickness; relaxation ratio will be changed by the growth temperature at the initial growth stage. I assumed that the thickness of the LT-ZnTe buffer layer is enough to accommodate the lattice misfit. But, there were several reports, that indicate that

when the thickness of LT-ZnTe buffer layer is too thick, the quality of overgrown film degrades fast [9].

Figure 3.2 shows the RHEED observation results of both samples: (a) sample-A and (b) sample-B. Initial nucleation mode (three-dimensional growth) appeared within a few minutes from both samples. Then a streaky pattern with a (2 x 1) reconstruction was observed during the whole growth process. Since the growth conditions were optimized, significant difference cannot be observed except that the sample-B shows relatively streaky RHEED patterns.



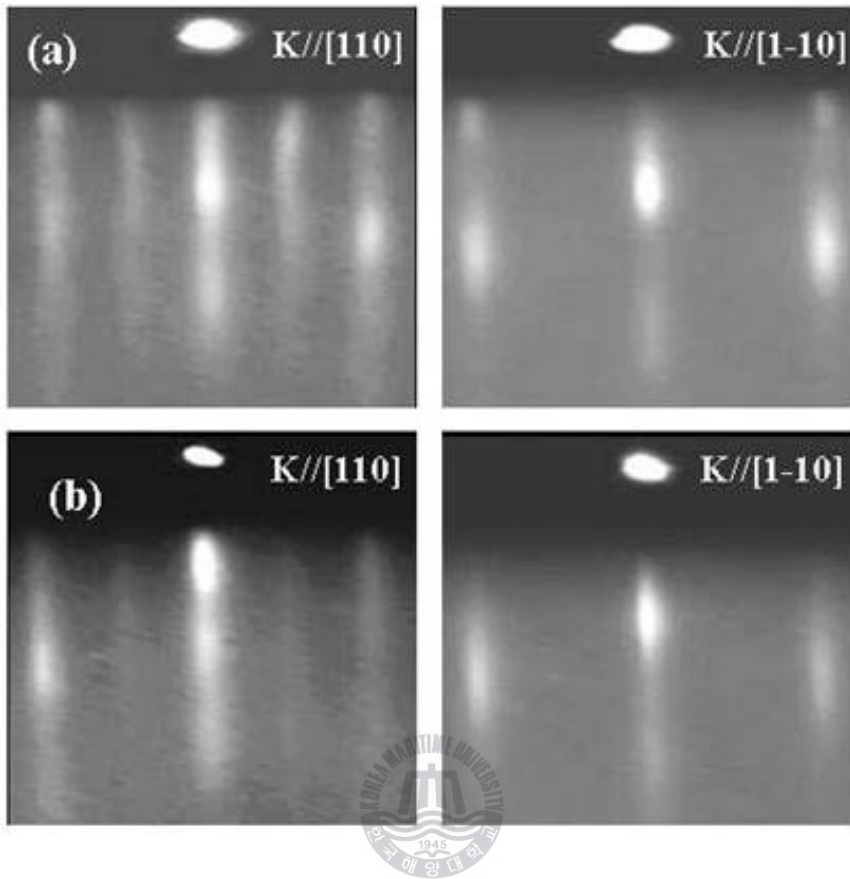


Figure 3.2 RHEED images of (a) sample-A (HT-ZnTe/GaAs) and (b) sample-B (HT-ZnTe/LT-ZnTe/GaAs)

3.4) Surface morphology

Figure 3.3 shows AFM images. Sample-A and sample-B shows root-mean-

square (RMS) roughness of 4.127, and 4.122 nm, from 10 x10 μm^2 area, respectively. Although the sample-B shows relatively small value, the difference was not considerably large as that which corresponds with the RHEED observation.

Surface smoothness is known as a function of growth temperature, grain size, growth rate and so on. Also it indirectly reveals the crystal quality of the film. Thus, the AFM results indicate that the crystallinity of both samples would not show large difference.

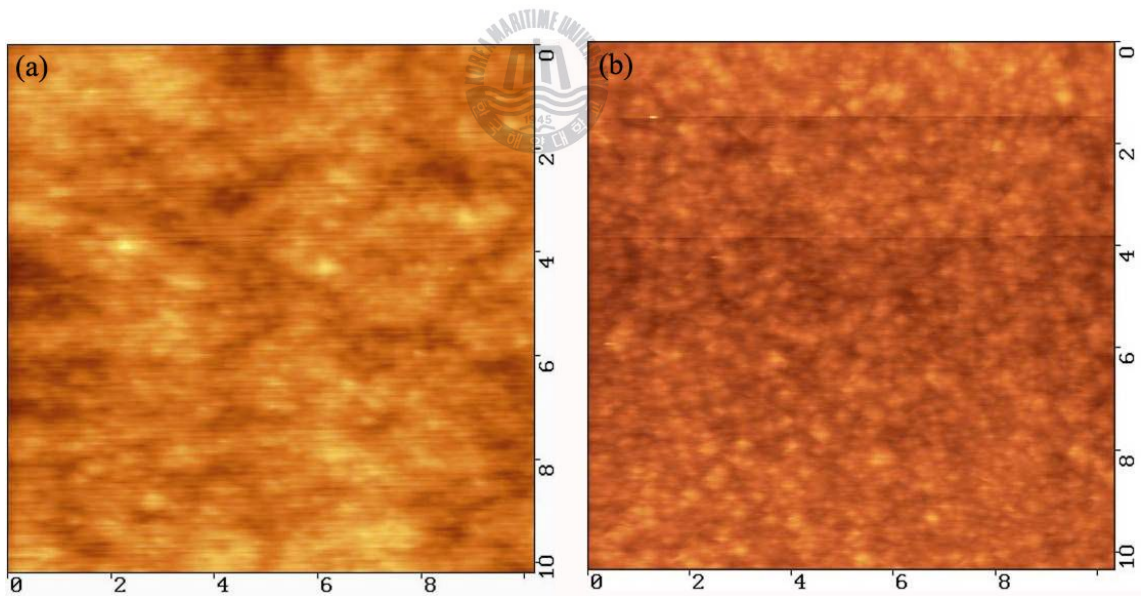


Figure 3.3 AFM images of (a) sample-A (HT-ZnTe/GaAs) and (b) sample-B (HT-ZnTe/LT-ZnTe/GaAS)

3.5) The investigation of crystallinity

Figure 3.4 shows ω and ω - 2θ scans of both samples. From both scans, sample-B shows relatively narrower linewidth than sample-A, but as expected above, large difference was not observed. The linewidth decreases from 260 to 247 arcsec in ω - 2θ scan and from 1236 to 1208 arcsec in ω scan, respectively. Based on these facts, I conclude that the sample-B has better crystallinity than sample-A. Although due to the thin layer thickness, the XRD linewidth is broader than that of previous report [1].



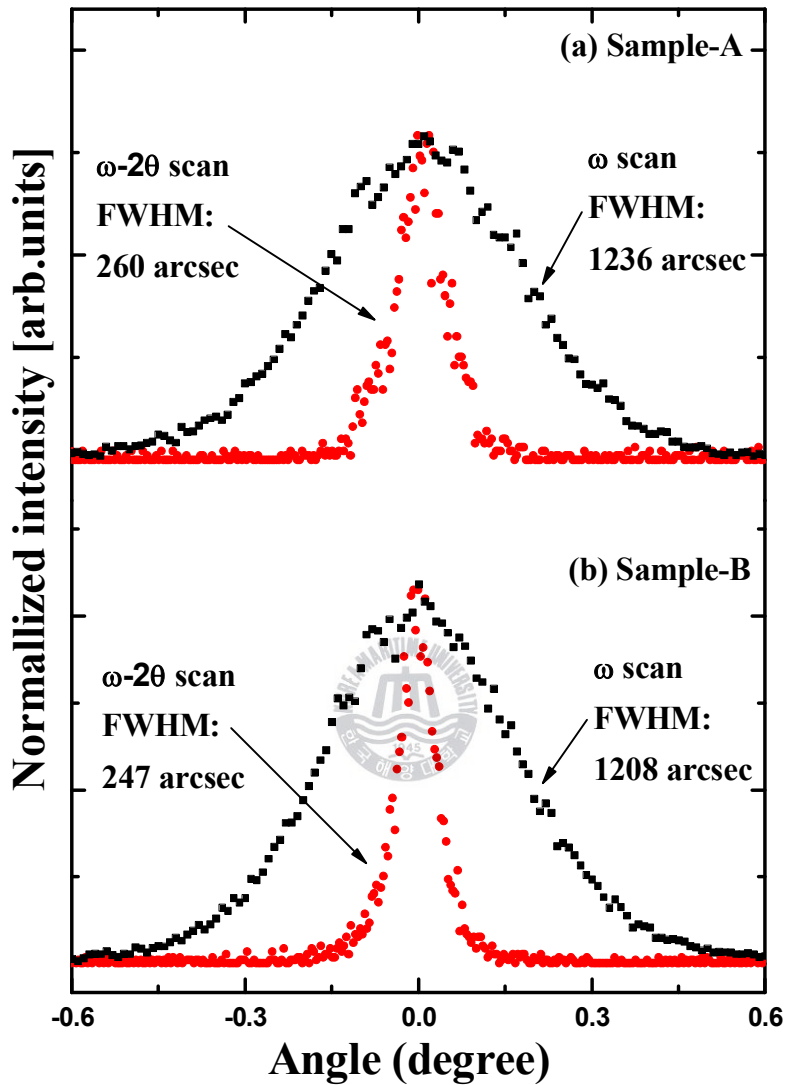


Figure 3.4 X-ray diffraction measurement results of (a) ω/ω -2 θ scan of sample-A (HT-ZnTe/GaAs) and (b) ω/ω -2 θ scan of sample-B (HT-ZnTe/LT-ZnTe/GaAS)

It is worth to consider about the various parameters that determine the XRD

linewidth. The linewidth of X-ray rocking curve reflects various factors such as rotation of mosaics, crystal size effect, local strain and defect density in the film. The measured linewidth of the XRD rocking curve can be explained numerically as [10]

$$\beta_{meas.}^2 = \beta_0^2(hkl) + \beta_d^2(hkl) + \beta_a^2(hkl) + \beta_\varepsilon^2(hkl) + \beta_L^2(hkl) + \beta_r^2(hkl) \quad (3.1)$$

where the β_0 is the intrinsic linewidth [9], the β_d is the intrinsic rocking curve width for the first crystal, the β_a is the linewidth due to angular rotation at the dislocations, the β_ε is the linewidth by the strain surrounding dislocations, the β_L is the term of crystal size effect, and the β_r is the bending effect. Among them, the layer thickness (β_L) and dislocation density in the layer (β_a , β_ε) may have dominant affect on the XRD linewidth of the ZnTe layers. In this experiment, since the layer thickness is the same, the improvement of crystallinity is deduced to the reduction of dislocation (grain boundary) density.

Also the surface-normal lattice constants are evaluated as 6.088 Å and 6.101 Å for sample-A and sample-B, respectively, from XRD (004) ω -2 θ scan. Sample-B shows the lattice parameter, which is very close to that of bulk ZnTe. Note that the lattice mismatch relaxation accompanies the dislocation generation. Therefore,

lattice misfit relaxation broadens the XRD linewidth of epitaxial layer. In our experiment, however, the sample-B has narrower linewidth than the sample-A, which strongly indicates that the LT-buffer accommodates lattice mismatch effectively.

3.6) Crystal deformation

Figure 3.5 shows reciprocal space mapping (RSM) results of ZnTe layers. The RSM result of sample-A indicates the misalignment between the reflection planes of grown film and substrate, while it was not observed from sample-B. Such a misalignment is known due to the monoclinic distortion or tilting, which originates from the partial relaxation of lattice strain.

These results imply that ZnTe layer without buffer suffers significant lattice deformation. It can be understood that since the LT-ZnTe buffer layer enhances lattice misfit relaxation, the layer grown on LT-buffer would have less strain. Therefore, the sample-B shows less deformation than sample-A.

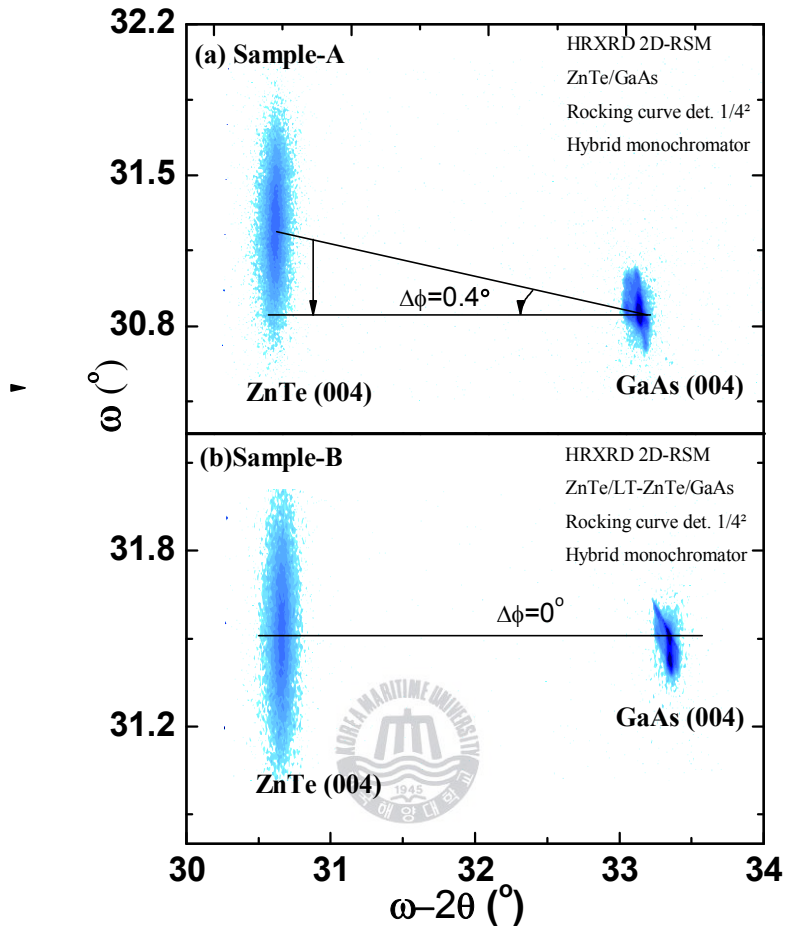


Figure 3.5 XRD reciprocal space mapping results of (a) sample-A (HT-ZnTe/GaAs) and (b) sample-B (HT-ZnTe/LT-ZnTe/GaAs)

The role of LT-ZnTe buffer described in this experiment can be summarized as follows (a) the reduction of misfit dislocation generation in the overgrown layer, (b) the enhancement of misfit relaxation and (c) the diminishment of the structural

deformation. Note that all these effects may improve the crystallinity of overgrown layer.

3.7) Conclusion

The effect of LT-buffer on the structural properties of high-temperature-grown ZnTe layers has been investigated. Structural deformation of ZnTe layer was reduced by using LT-buffer and the role of LT-buffer layer is found to be the following: the reduction of misfit dislocation generation and the diminishment of the structural deformation in the overgrown layer due to the fast misfit relaxation during the growth of LT-buffer.



Reference

- [1] J.H. Chang, K. Goto, J.S. Song, D.C. Oh, C.W. Lee, T. Yao, *J. Crystal Growth* 251, 596 (2003)
- [2] H. Amano, N. Sawaki, Y. Toyoda, *Appl. Phys. Lett.* 48 (5), 353 (1986)
- [3] V.I. Kozlovsky, A.B. Kryso, Yu.V. Korostein, Yu.G. Sadofyev, *J. Crystal Growth* 214-215, 35 (2000)
- [4] R. Droopad, Z. Yu, C. Overgaard, J. Edwards, J. ramdani, L. Hilt, J. Curless, J. Finder, K. Eisenbeiser, A. Demkov, B. Ooms, *Appl. Phys. Lett.* 80 (10), 1803 (2002)
- [5] K. Kanisawa, H. Yamaguchi, Y. Hirayama, *Appl. Phys. Lett.* 76 (5), 589 (2000)
- [6] J.S. Song, J.H. Chang, S.K. Hong, M.W. Cho, H. Makino, T. Hanada, T. Yao, *J. Crystal Growth* 242, 95 (2002)
- [7] V.H. Etgens, M. Sauvage-Simkin, R. Pinchaux, J. Massies, N. Jedrecy, A. Waldhauer, S. Tatarenko, P.H. Jouneau, *Phys. Rev. B* 47, 10607 (1993)
- [8] S.G. Nam, Y.M. Yu, J.K. Rhee, B.S. O, Y.D. Choi, J.W. Lee, Y.J. Jung, *Mater. Chem. Phys.* 69, 30 (2000)
- [9] S.D. Wu, L.W. Guo, Z.H. Li, X.Z. Shang, W.X. Wang, Q. Huang, J.M. Zhou, *J.*



Crystal Growth 277, 21 (2005)

[10] J.E. Ayers, J. Crystal Growth 135, 71 (1994)



Chapter 4. MBE growth of GaSb films by using three-steps ZnTe buffer layer

4.1) Introduction

The GaSb-based compound semiconductors have great potential for various military and civilian applications such as laser diodes, photo-detectors and high-frequency electronic devices. Therefore, numerous efforts have been made to grow high quality GaSb and related compounds. However, the crystal quality of GaSb has been restricted due to the large lattice mismatch to the conventional substrates. A lot of approaches have been tested to solve the problem [1-7]. Usually, a buffer layer with graded or staircase composition profile is adopted to grow high-quality GaSb heteroepitaxy [2]. However, cumbersome and time-consuming process with highly accurate control of growth conditions is required to improve the crystallinity of the heteroepitaxial layer. Therefore, it is inevitably required to develop a new buffer layer growth technique.

In this chapter, a three-step ZnTe buffer layer is introduced for the growth of a high-quality GaSb layer. Since ZnTe ($L_C = 6.104 \text{ \AA}$) has a very close lattice

constant to GaSb ($L_C = 6.095 \text{ \AA}$), it is regarded as one of the best buffer layer for GaSb growth. Also, the role of the buffer layer, especially for the structural quality of GaSb layers, has been discussed by using reciprocal space mapping (RSM) results.

4.2) Experimental details

For the MBE growth, GaAs (001) substrates were degreased and etched by using NH_4OH solution. Then it was mounted on a Mo holder using In. Thermal treatment was performed at $640 \text{ }^\circ\text{C}$ for 15 min in ultra high vacuum (UHV). During the thermal treatment (4×2), reconstruction pattern was observed. The reflection high energy electron diffraction (RHEED) pattern was almost streaky at the end of thermal treatment.

Two samples were prepared for this chapter: sample-A is GaSb/GaAs and sample-B is GaSb/HT-ZnTe/LT-ZnTe/GaAs. To highlight the effect of the buffer layer, both samples were grown at the same growth conditions except for the existence and nonexistence of the buffer layer. The growth of GaSb was performed at $540 \text{ }^\circ\text{C}$, and the thickness of the GaSb layer was controlled to 500 nm. The

growth rate was optimized to 300 nm/h for ZnTe and to 500 nm/h for GaSb layers, respectively. Flux ratio was controlled at ~ 2 (VI/II) for ZnTe and at ~ 5 (V/III) for GaSb, respectively.

The three-step buffer was grown in following way: (the first step) thin (~ 30 nm) low-temperature buffer (LT-buffer) was grown at 250 °C, then (the second step) high-temperature annealing was performed at 330 °C for 30 min, finally (the third-step) a relatively thick (300 nm) high-temperature buffer (HT-buffer) was grown at 310 °C. After finishing the three-step buffer growth, GaSb layers were grown at 540 °C.



The LT-ZnTe buffer layer is introduced to minimize the defect generation at the ZnTe-GaAs heterovalent interface. Annealing of the LT-ZnTe buffer layer is employed to terminate the threading dislocation, also the HT-ZnTe buffer layer is employed a smooth surface for two-dimensional GaSb growth.

During the growth, RHEED pattern was observed. High-resolution X-ray diffraction measurement (HRXRD) was used to evaluate the structural quality of the samples. The surface morphology was observed by atomic force microscopy (AFM). Reciprocal space mapping (RSM) was used to observe the structural

deformation of the GaSb layers.

4.3) Surface observation

Figure 4.1 shows the RHEED patterns observed during the growth. In the case of sample-A, the initial growth mode is very similar to that of ZnTe/GaAs due to the similar lattice mismatch (+7.8 %). As shown in Figure 4.1 (a), the growth was initiated from three-dimensional (3D) growth, then after a few minutes, the growth mode was changed into 2D growth. During the growth, a (1 x 3) reconstruction pattern was observed.



But the growth of sample-B shows a remarkable difference from sample-A. The initial 3D growth was not observed and the RHEED pattern during the growth was streaky and (1 x 3) reconstruction pattern from the very beginning of the growth.

Note that the lattice misfit of GaSb/GaAs substrate is 7.8 %, while it is just 0.14 % for GaSb/ZnTe buffers. Generally, the 0.14 % misfit can be accepted as a nearly lattice-matched condition [8]. Therefore, initial 3D growth was not observed during the growth of GaSb/ZnTe buffer.

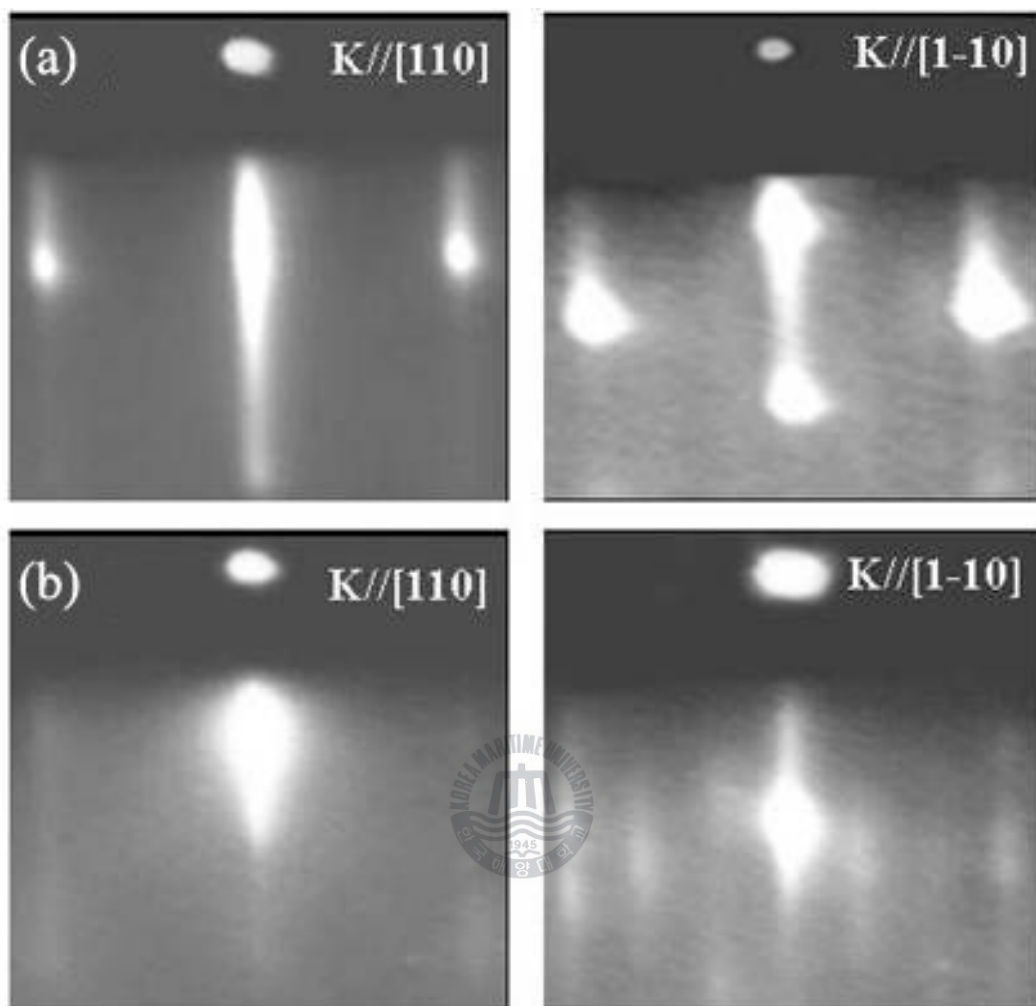


Figure 4.1 RHEED images of (a) sample-A (GaSb/GaAs) and (b) sample-B (GaSb/ZnTe buffer/GaAs)

4.4) Surface morphology

Figure 4.2 shows AFM images. As one can expect from the RHEED observation results, sample-B shows a much smoother surface morphology than

sample-A. Sample

-A shows rough surface with a root-mean-square (RMS) roughness of 107 nm from $10 \times 10 \mu\text{m}^2$ area. But sample-B shows a very smooth surface with an RMS roughness of 3.3 nm from the same observation area.

The difference could be understood in terms of the difference of an initial growth mode. Sample-B should have a smooth surface, because it was grown without 3D mode even at the initial stage. Once the 3D growth initiates, the migration length of adatom will be decreased and the surface will be roughened. Thus, the remarkable difference of surface morphology can be deduced to the growth mode difference, which is provided by the ZnTe buffer.

Also, surface smoothness is known as a function of growth temperature, grain size, growth rate and so on. Since large size means smooth surface, it indirectly reveals the crystal quality of the film. Therefore, improvement of structural quality is expected from sample-B.

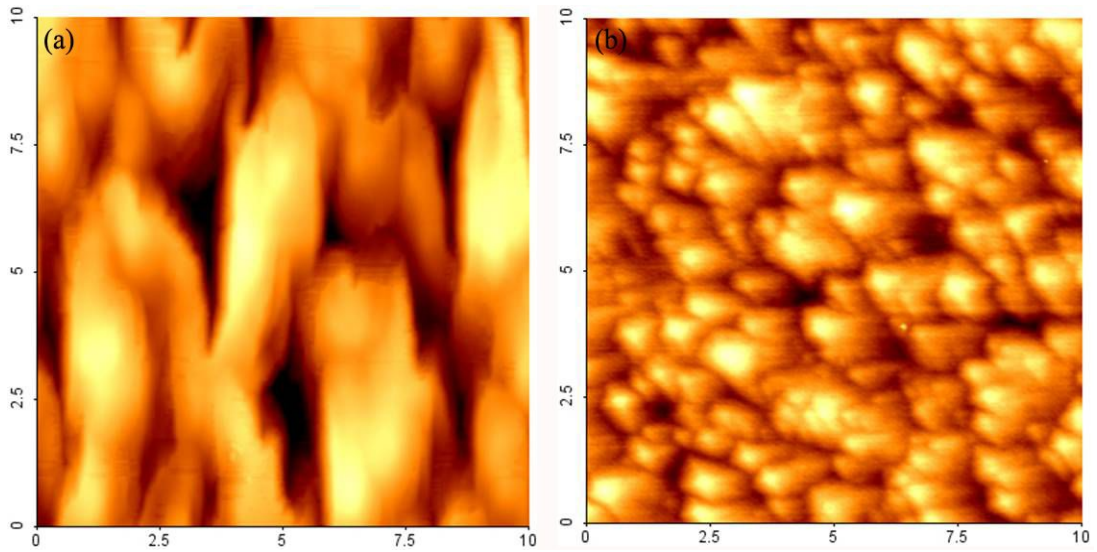


Figure 4.2 AFM images of (a) sample-A and (b) sample-B



4.5) Crystallinity improvement

Figure 4.3 shows XRD ω - and ω -2 θ scans of GaSb layers (sample-A and -B). The linewidth decreases from 177 to 171 arcsec in ω -2 θ scan. But drastic decrease is observed in ω scans. It decreases from 1154 to 606 arcsec. If one considers the large lattice mismatch between GaSb and GaAs, the narrow XRD linewidth of sample-B clearly demonstrates the improvement of crystal quality by the ZnTe buffer layer.

Note that the XRD linewidth of sample-B is comparable to the reported value

[9], which is 582 arcsec MBE grown GaSb film with 500 nm-thick, although the growth conditions was not optimized yet. In this chapter, since the layer thickness was the same, the improvement of XRD linewidth is deduced to the reduction of dislocation (grain boundary) density.

Also the surface-normal lattice constants are evaluated as 6.118 Å (sample-A) and 6.098 Å (sample-B) from the (004) ω -2 θ X-ray rocking curve, respectively. Sample-B has the lattice parameter, which is very close to that of bulk GaSb lattice constant, while considerable residual strain observed from sample-A. The residual strain is estimated as -0.377% and -0.0949% for sample-A and -B, respectively.

Note that the lattice mismatch relaxation accompanies the dislocation generation. Therefore, lattice misfit relaxation broadens the XRD linewidth of the epi-layer. However, sample-B has a narrow XRD linewidth than sample-A; this fact strongly indicates that the ZnTe buffer is effective for the accommodation of lattice mismatch.

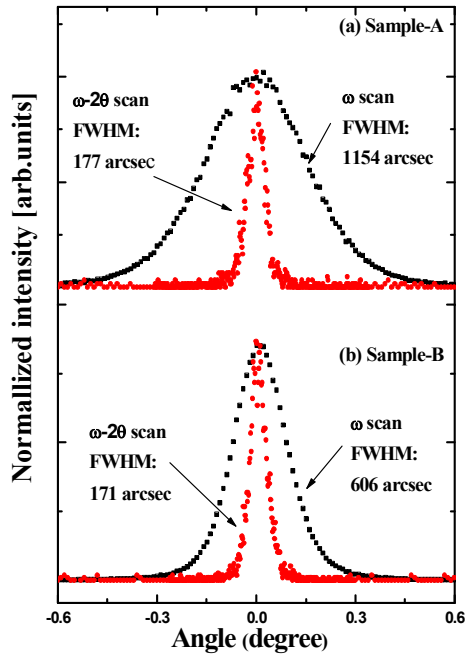


Figure 4.3 X-ray diffraction measurement results of (a) ω/ω -2 θ scan of sample-A and (b) ω/ω -2 θ scan of sample-B

4.6) Structural deformation

Figure 4.4 shows reciprocal space mapping (RSM) results of GaSb layers. The RSM result of sample-A shows significant misalignment as large as 0.1° , while it is diminished to 0.025° from sample-B. Such a misalignment is known due to the monoclinic distortion or tilting, which originates from the partial relaxation of lattice strain. The result implies that the ZnTe buffer is a successful template for the

growth of GaSb.

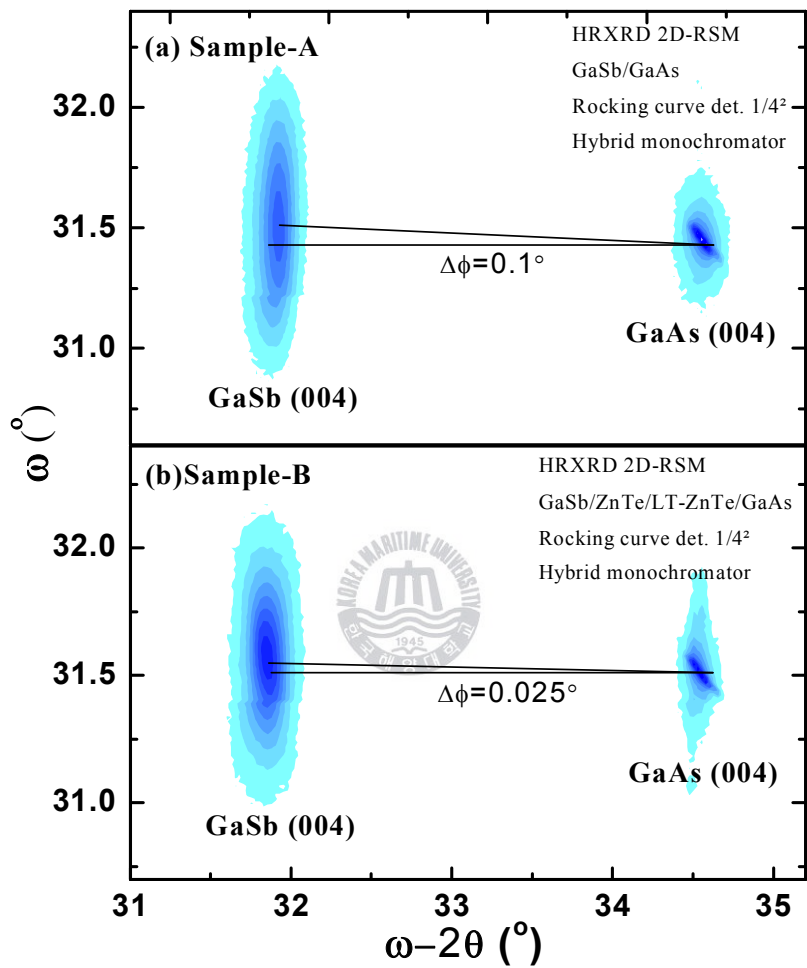


Figure 4.4 X-ray diffraction reciprocal space mapping results of (a) sample-A and (b) sample-B

The effects of the three-step ZnTe buffer described in this experiment can be summarized as follows: (a) the efficient accommodation of the large lattice misfit, (b) providing smooth surface for the following layers, (c) the reduction of residual strain (of course, it is very closely related with the relaxation of lattice misfit) and (d) the diminishing of the structural deformation due to incomplete relaxation of strain.

These effects can be understood through the consideration of the role of the three-step buffer. It was reported that the accommodation of lattice misfit is mainly accomplished by the LT buffer [6].  During the growth of the LT buffer, high-density misfit dislocations are generated by the relaxation of lattice mismatch. These dislocations are terminated by making loop or bending during the annealing; thus the annealing process is indispensable for the growth of high-quality HT buffer with low dislocation density. Therefore, it can be concluded that the role of a three-step ZnTe buffer is really essential for the remarkable improvement of GaSb layer quality in terms of providing high-quality substrate.

4.7) Conclusion

Remarkable improvement of crystal quality of GaSb heteroepitaxial layer is achieved by inserting a three-step ZnTe buffer. The effect of ZnTe buffer to the structural properties of GaSb layers has been investigated. By using the three-step ZnTe buffer, smooth surface morphology, narrow rocking curve linewidth and the reduction of residual strain in the GaSb layer have been achieved. It is concluded that the ZnTe buffer layer is really effective for the accommodation of the misfit to grow high-crystalline GaSb layer.



Reference

- [1] N. Yahyaoui, S. Aloulou, R. Chtourou, A. Sfaxi, M. Oueslati, *Appl. Surf. Sci.* 253 (2006) 292.
- [2] H. Amano, N. Sawaki, I. Akasaki, Y. Toyoda, *Appl. Phys. Lett.* 48 (5) (1986) 353.
- [3] R. Droopad, Z. Yu, C. Overgaard, J. Edwards, J. Ramdani, L. Hilt, J. Curless, J. Finder, K. Eisenbeiser, A. Demkov, B. Ooms, in: V. Shutthanandan, S. Thevuthasan, Y. Ling, E.M. Adams, R. Droopad, (Eds.), *The Eighth Workshop on Oxide Electronics*; *Appl. Phys. Lett.* 80 (10) (2002) 1803.
- [4] K. Kanisawa, H. Yamaguchi, Y. Hirayama, *Appl. Phys. Lett.* 76 (5) (2000) 589.
- [5] J.S. Song, J.H. Chang, S.K. Hong, M.W. Cho, H. Makino, T. Hanada, T. Yao, J. *Crystal Growth* 242 (2002) 95.
- [6] J.H. Chang, K. Godo, J.S. Song, D.C. Oh, C.W. Lee, T. Yao, J. *Crystal Growth* 251 (2003) 596.
- [7] S.G. Nam, Y.M. Yu, J.K. Rhee, B.S. O, Y.D. Choi, J.W. Lee, Y.J. Jung, *Mater. Chem. Phys.* 69 (2001) 30.
- [8] T. Yao, T. Takeda, *Appl. Phys. Lett.* 48 (1986) 160.

[9] K. Akahane, N. Yamamoto, S.I. Gozu, N. Ohtani, J. Crystal Growth 264 (2004)

21.



Chapter 5. MBE growth of GaSb films; The influence of the chemical composition of ZnTe surface

5.1) Introduction

In the previous chapter 3, ZnTe ($L_c = 6.104 \text{ \AA}$) buffer have been suggested as a new buffer layer for the growth of GaSb on GaAs, and the growth of the high-quality GaSb was achieved by using three-step ZnTe buffer layer in chapter 4. However, the influence of GaSb/ZnTe heterointerface didn't be considered systemically. Note that the GaSb/ZnTe hetero-interface contains unstable bonds such as Zn-Sb and Te-Ga. It implies that the crystal quality of overgrown layer will be greatly influenced by the interface chemistry like as the ZnSe/GaAs hetero-interface in which preventing Ga-Se bond has been known as a key point to improve the ZnSe quality [1-4]. In this chapter, the crystallinity of GaSb has been optimized in terms of II-VI/III-V hetero-interface.

5.2) Experimental details

All samples were grown by solid-source molecular beam epitaxy (MBE). The

thickness of GaSb layers directly grown on GaAs substrates was controlled to 1.4 μm . While it was controlled to be 0.4 μm in the case of grown on thick ZnTe buffers of 0.3 μm . The respective growth rate was 600 nm/h for ZnTe and 700 nm/h for GaSb layers. Flux ratio was ~ 2 (VI/II) for ZnTe and ~ 5 (V/III) for GaSb, respectively. ZnTe buffers were grown at 300 $^{\circ}\text{C}$, however in order to find out the optimum growth condition, GaSb layers were grown at the elevating temperatures (460 \sim 540 $^{\circ}\text{C}$).

To highlight the effect of surface composition, two samples were prepared with other treatment of ZnTe surface; sample-A was grown on Zn-terminated ZnTe surface and sample-B was grown on Te-terminated ZnTe surface. During the growth, RHEED pattern was observed to monitor the growth. High resolution X-ray diffraction measurement (HR-XRD) was used to evaluate the structural quality of the samples. The surface morphology was observed by atomic force microscopy (AFM).

The cathodoluminescence (CL) measurement were performed from 20K to room temperature by using liquid helium with temperature controller. The CL system was installed in a scanning electron microscope (HITACHI-S4200) with a

beam blanking system. The excitation energy and current were 10 kV and 3.5 nA, respectively. The electron range, which is measure of the range of electron-hole pair generation in the specimen, is calculated according to the formula given by Kanaya and Okayama [5]. The light was collected with an ellipsoidal mirror and led by an optical fiber to detection unit, and the monochromator was used to record. CL spectrum was detected by photomultiplier (Hamamatsu; H10330-75)

5.3) Growth temperature optimization

Large lattice mismatch in GaSb/GaAs system (+ 7.8 %) will be relaxed just after the growth start. Once the relaxation begins, it accompanies high-density dislocation which causes difficulty for the exact evaluation of hetero-interface. Therefore, the growth of GaSb on GaAs substrate is optimized to magnify the influence of hetero-interface.

Figure 5.1 shows the evolution of the surface roughness and the HR-XRD full width at half maximum (FWHM) values depending on the GaSb growth temperature. The thickness of each GaSb layer is fixed to 1.4 μm . As shown in figure 5.1, both surface roughness and HR-XRD FWHM monotonically decrease

as increasing the growth temperature up to 525 °C. However, when the growth temperature increases higher, surface roughness and HR-XRD FWHM deteriorate. At the optimum growth temperature (~ 525 °C), the HR-XRD FWHM value of (004) ω -2 θ scans is 352 arcsec, and the root-mean-square (RMS) roughness is ~1.2 nm. Note that both surface roughness and XRD linewidth varies similarly. As the growth temperature increasing, smooth surface is obtained owing to the migration length increasing of adsorbed atoms (adatom) on the surface. Since MBE is a kinetic process which happens under almost non-equilibrium condition, thus smooth surface enhances two-dimensional (2D) growth and resultantly improves the crystallinity of film. While when the growth temperature is too high, desorption of adatom increases, which sometimes degrades the quality of film significantly. The degradation of crystallinity at high growth temperature is known to be mainly originated from the increase of Sb-desorption [6]. When the Sb-desorption increases, V/III ratio decreases, and the crystallinity degrades due to the collapse of stoichiometry in the film.

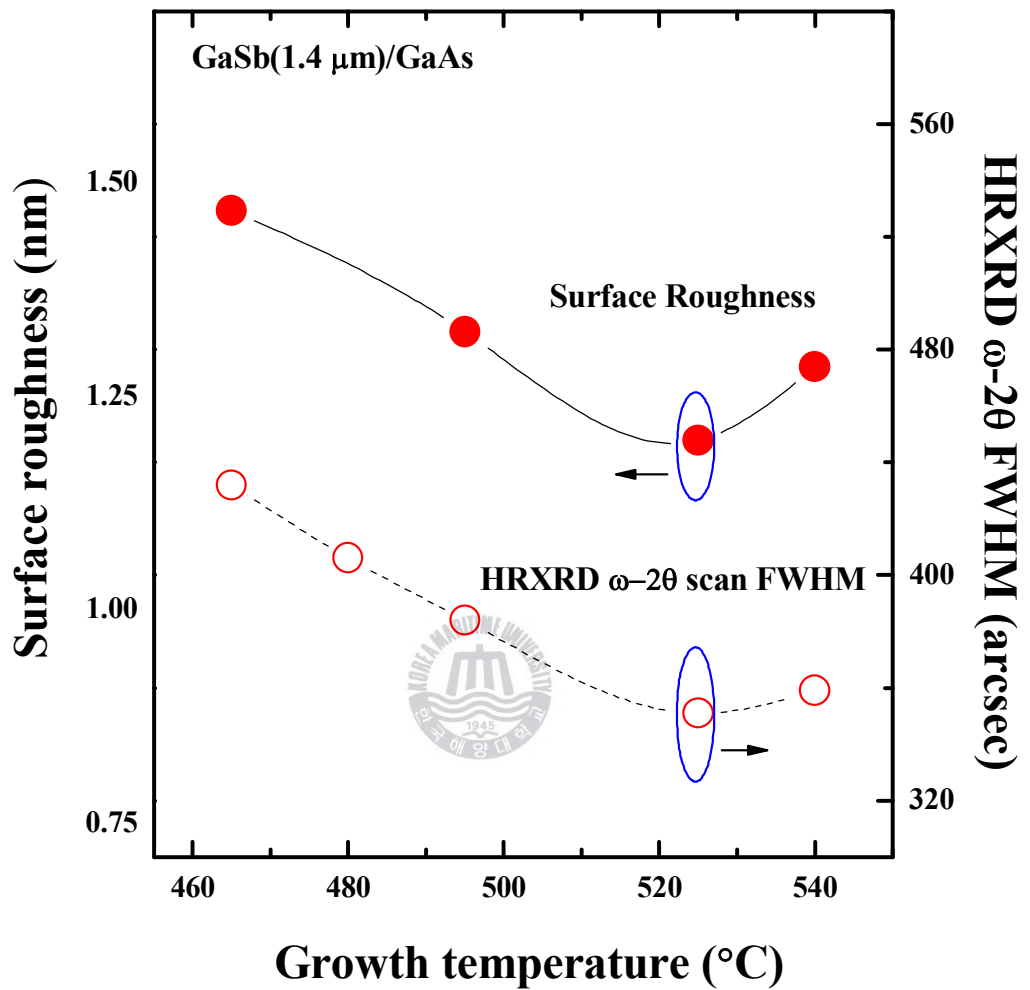


Figure 5.1 Growth temperature dependence of GaSb/GaAs layers. The surface roughness and HRXRD linewidth is optimized at 525 °C.

5.4) RHEED observation by interface composition

Two distinct bonds are expected during the growth of GaSb on ZnTe. One is Ga–Te bond, another is Zn–Sb bond. The reaction of Ga and Te results in the formation of a Ga_2Te_3 . Generally, it contains a lot of cation vacancies, therefore the crystallinity of overgrown film degrades [7]. While, as a result of the reaction between Zn and Sb, Zn_3Sb_2 - like structure is expected. Although, details on Zn_3Sb_2 were not known, that structure was estimated that it has similar physical properties with Zn_3N_2 , which has anti-bixbyite structure with anion vacancies [8]. Therefore, both interfacial structures have negative effect to the high quality GaSb film growth.

Two samples were prepared to highlight the influence of interface chemistry. Sample-A is GaSb grown on Zn-terminated ZnTe surface, and sample-B is a GaSb grown on Te-terminated ZnTe surface. Zn (Te)-terminated surface was achieved by Zn (Te) flux exposure onto the ZnTe surface for 10 min at 300 °C. The surface chemistry was confirmed by the RHEED reconstruction patterns. The optimum growth temperature of GaSb is too high to keep the intended surface, therefore GaSb growth was started at low temperature (300 °C), and after short (2 min) growth, the growth interrupted to increase the growth temperature to 525 °C then

proceeded again to grow 0.4- μm thick GaSb films.

Figure 5.2 shows the RHEED patterns observed during the growth. Figure 5.2a–c show RHEED patterns obtained from sample-A. Figure 5.2a shows a $c(2 \times 2)$ Zn-reconstructed surface. The surfaces were almost streaky and when the growth was started of GaSb, 3-dimensional (3D) feature was not observed as shown in figure 5.2b, while figure 5.2d–f show RHEED images during the growth of sample-B. Figure 5.2d shows a (2×1) Te-reconstructed surface. The surface was almost smooth, but 3D growth was obviously observed at the initial growth stage (figure 5.2e), which just continued less than a few tenth of seconds (< 10 nm). It should be noted that an extra spots indicating the existence of different structural phase were not observed, which makes me exclude the possibility of considerable alloying at the interface.

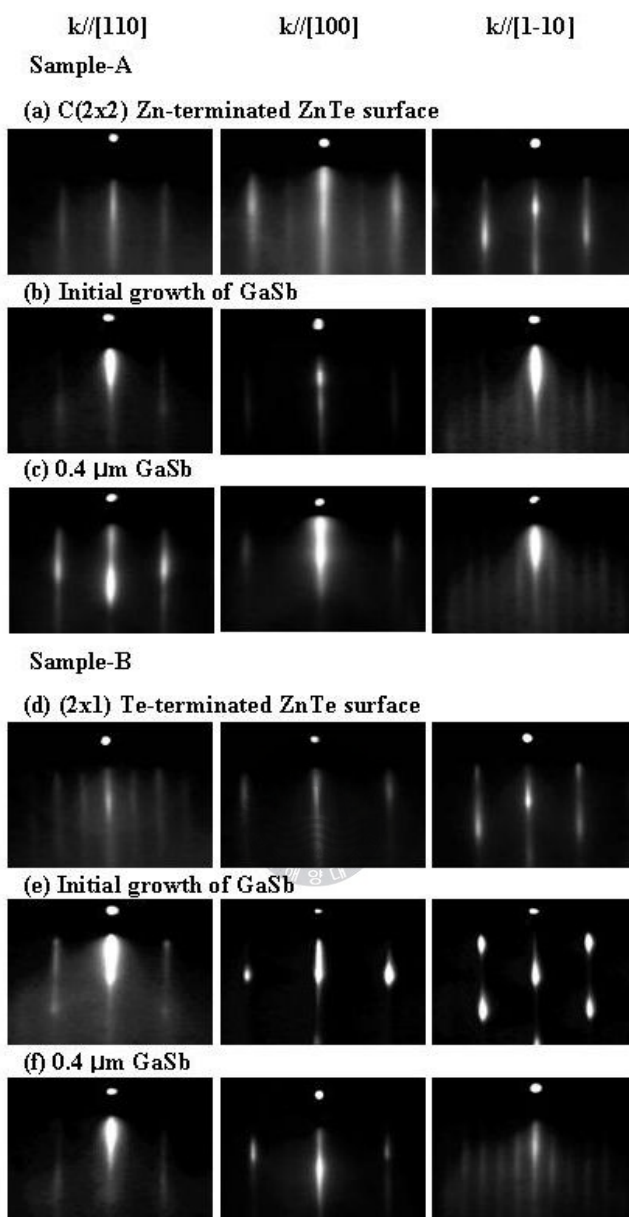


Figure 5.2 RHEED patterns of sample-A (GaSb/Zn-terminated ZnTe) (a) c(2 x 2) Zn-terminated ZnTe surface, (b) initial growth of GaSb, (c) 0.4 mm GaSb; sample-B (GaSb/Te-terminated ZnTe) (d) (2 x 1) Te-terminated ZnTe surface, (e) initial growth of GaSb, (f) 0.4 mm GaSb.

To understand the RHEED evolution for each sample, the surface chemistry of the surfaces have been considered, because the probability of unwilling interfacial structure might be mainly determined by the surface coverage and formation energy of chemical bond for each surface. First of all, the Zn-coverage of $c(2 \times 2)$ surface is known to be half-monolayer (ML) [9], while Te-coverage on (2×1) surface is believed to be almost unity [9]. Therefore, Te-terminated surface will make larger influence on the GaSb than Zn-terminated surface, under the assumption of similar bonding strength for Ga–Te and Zn–Te bonds. Although, reliable report on Zn–Sb bond is lacking, chemical bonding strength is able to be estimated by the bonding length for each bond. The respective covalent radii for Zn–Sb bond and Ga–Te bond is estimated to be 0.267 nm and 0.258 nm, based on the reported tetrahedral covalent radii [10]. It implies that Ga–Te bond has higher probability than that of Zn–Sb bond. The discussion on both surface coverage and bonding length predicts that interfacial layer is more presumable for Te-terminated surface. It corresponds with the RHEED observation results (figure 5.2). Note that, when a film begins to grow on a surface with low surface energy, 3D growth is preferred to decrease Gibbs total energy in the film [11]. In this experiment, lattice

mismatch is negligible due to negligible small lattice mismatch (0.14 %) between GaSb and ZnTe, hence 3D growth during the initial growth of GaSb should be deduced to the formation of interfacial layer. Therefore, the 3D growth during the initial growth stage of sample-B (GaSb/Te-terminated ZnTe) was attributed to the low surface energy of interfacial layer, which indicates that Zn-termination is desirable to diminish the influence of interface layer.

5.5) Surface morphology

Figure 5.3 shows AFM images of (a) sample-A and (b) sample-B. As expected from the RHEED observation results, sample-A shows smaller surface roughness (RMS = 1.42 nm) than sample-B (RMS = 1.82 nm). Sample-B reveals a typical morphology of 3D growth, which coincides with the RHEED observation results as shown in figure 5.2. Surface roughness is known to be determined by growth temperature, grain size, and growth rate. Since large grain size means smooth surface, it indirectly reveals the crystal quality of the film. Therefore, high structural quality is expected from the sample-A due to the smooth surface corresponding to the RHEED images.

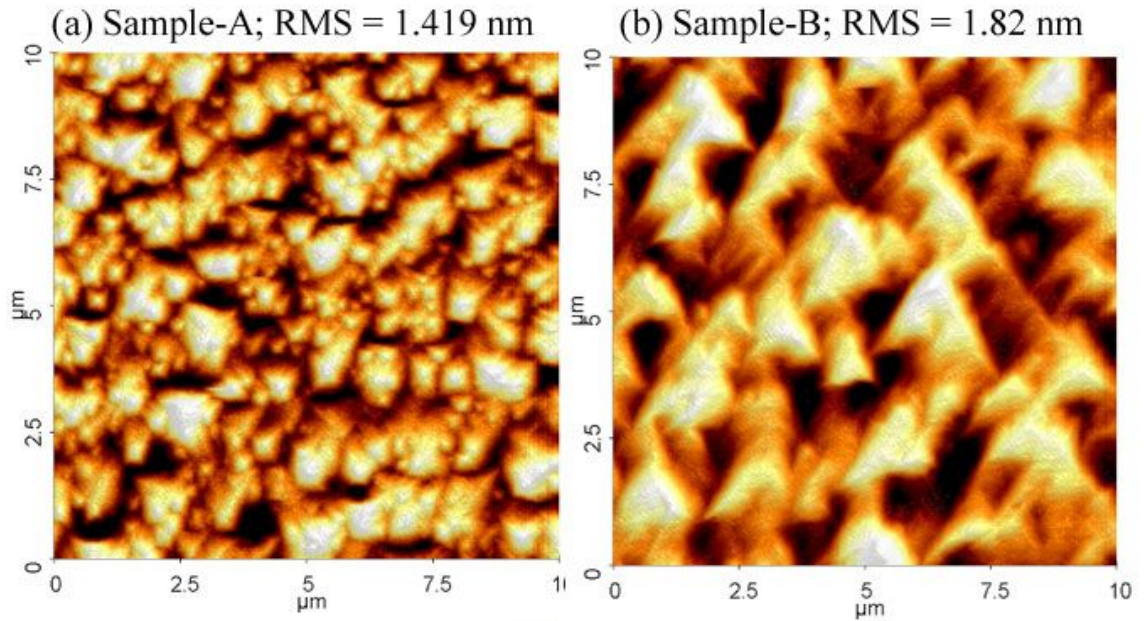


Figure 5.3 AFM images of (a) sample-A (GaSb/Zn-terminated ZnTe, RMS = 1.419 nm) and (b) sample-B (GaSb/Te-terminated ZnTe, RMS = 1.82 nm).

5.6) Evaluation of structural characterization by interface composition

Figure 5.4 shows (004) ω -2 θ scans of GaSb films. Figure 5.4a and b show HR-XRD results of GaSb layers grown on ZnTe buffer (sample-A and sample-B), respectively, while figure 5.4c is a result of GaSb directly grown on GaAs substrate. Sample-A and sample-B reveals XRD FWHM of 113 arcsec and 163 arcsec, respectively, but sample-C reveals relatively broad FWHM as broad as 352 arcsec.

Considerable improvement of crystallinity in terms of XRD FWHM is obvious for GaSb/ZnTe samples. Also sample-A shows narrow XRD FWHM than sample-B. Remind that the growth on Te-terminated surface accompanies 3D growth (sample-B), hence GaSb growth on Te-terminated surface shows broader HRXRD linewidth in compare to sample-A. It reveals strongly that Zn-terminated ZnTe surface is useful for the high quality GaSb growth.

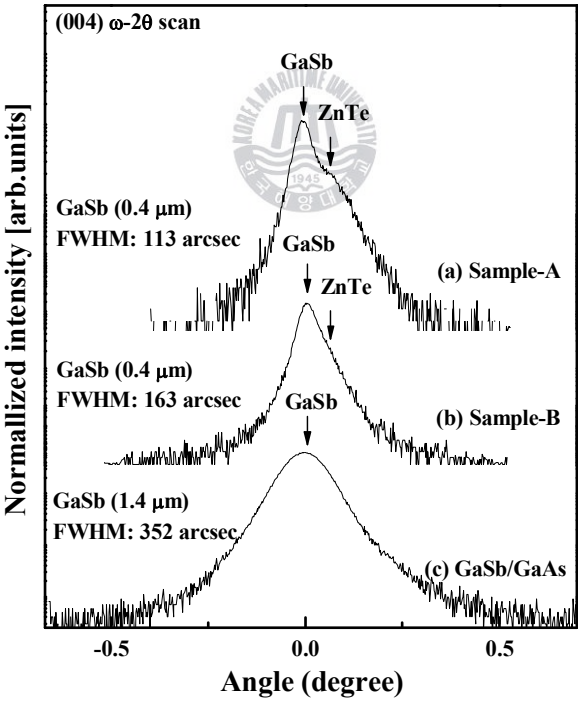


Figure 5.4 XRD (004) ω -2 θ scan of (a) sample-A (GaSb/Zn-terminated ZnTe), (b) sample-B (GaSb/Te-terminated ZnTe) and (c) GaSb/GaAs.

Table 5.1 Lattice constant, residual strain and relaxation ratio of GaSb layers grown on GaAs substrates with/without ZnTe buffer

Sample No.	GaSb thickness	Lattice constant	Residual strain (ϵ)
Sample-A (Zn-termination)	0.4 μm	6.096 \AA	- 0.0164 %
Sample-B (Te-termination)	0.4 μm	6.101 \AA	- 0.0984 %
GaSb without buffer (525 $^{\circ}\text{C}$ growth)	1.4 μm	6.1078 \AA	- 0.21 %



To consider the structural properties in detail, lattice constant, residual strain, and relaxation ratio of those samples are listed in table 5.1. The respective surface-normal lattice constants are evaluated to be 6.096 \AA (sample-A), 6.101 \AA (sample-B) and 6.108 \AA (GaSb/GaAs) from the (004) ω -2 θ scan. Note that sample-A has both the narrowest XRD FWHM and smallest residual strain, which is paradoxical result. Generally, it indicates that XRD linewidth broadens as a function of inhomogeneous strain induced by imperfection of crystal, thus small linewidth means low defect density in the film. However, residual strain in a heteroepitaxial

film is generally decreased by the relaxation of mismatches. In generally, fully relaxed film contains higher dislocation density than strained film. Moreover, sample-A (0.4 μm) is even thinner than GaSb (1.4 μm) film grown without ZnTe buffer. When the films are prepared under the same conditions, crystal size effect predicts that thinner film will have broad XRD linewidth [12]. Therefore small residual strain and narrow HRXRD linewidth for sample-A strongly indicate the availability of ZnTe buffer. Consequently, it is concluded that Zn-terminated surface provides optimum surface for the growth of high-quality GaSb films.



5.7) Low temperature cathodoluminescence properties.

In previous section (5.1 ~5.4), Zn-terminated ZnTe surface for GaSb growth selected for GaSb growth to obtain high quality GaSb layers and the interface quality was proved in terms of surface morphology and structural property. However, the luminescence properties were not investigated. Its investigation required for the optical application. Therefore, the low temperature (20 K) CL spectrum of sample-A (GaSb layers grown on Zn-treated ZnTe buffer layer) is shown in figure 5.5. A strong emission at 0.775 eV with a FWHM of 33.56 meV is

attributed to the radiative recombination by native acceptor level [13].

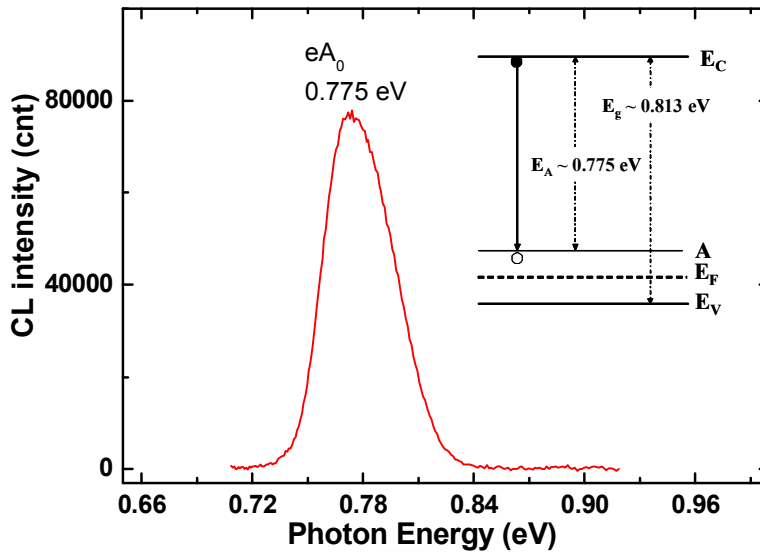


Figure 5.5 Cathodoluminescence spectrum of GaSb/Zn-terminated ZnTe at 20 K.

The inset is an energy diagram for the conduction band to neutral acceptor transition (eA_0)

The eA_0 is known to be associated with a native acceptor (as shown in the inset of figure 5.5) and evidence for this native acceptor appears in spectra of GaSb grown by all of the major growth techniques. The acceptor is intrinsic, and has been shown by Van der Meulen [14] to be a gallium vacancy-gallium antisite

complex (V_{Ga} , Ga_{Sb}). The inset of figure 5.5 explains the origin of luminescence by native acceptor level. At low temperature (5K) the Fermi level is below the acceptor level, which is therefore not occupied by an electron and is thus neutral. Luminescence transitions proceed from neutral donor levels to neutral acceptor levels, and at the higher temperatures (15 K ~), it changes into the transition from the conduction band to the native neutral acceptor levels [15].

5.8) Temperature dependence CL properties

This assignment of eA_0 by native acceptor level is demonstrated clearly in figure 5.6 (a) and (b) where they were plotted as a function of temperature from 20 K to 300 K.

As increasing the temperature, the intensity of eA_0 was attenuated and quenched in figure 5.6 (a). Also, the temperature dependence of CL emission peak position does not shrink monotonically. Generally, the peak position variation is not shifted nearly until 100 K then it moved exponentially to the low energy with increasing temperature. But, in this experiment, the peak position shows the red-shift from 20 K to 60 K, and it moved to the higher energy (blue-shift) from 60 K presumably

due to the thermal activation of eA_0 emission.

To validate the thermal activation of eA_0 , the temperature dependence of the integrated intensity of the 775 meV peak is shown in figure 5.6 (b). It is clear from data in figure 5.6 (a) that the temperature dependence of the 775 meV excitonic line can be divided into two distinct regions having very different slopes. The activation energy ΔE was fitted by using the Arrhenius equation (5.1) [16]:

$$I(T) = I_0 / [1 + C \exp(\Delta E / k_B T)] \quad (5.1)$$

I_0 is a constant related with internal luminescence efficiency, C is the ratio of nonradiative transition probability, k_B is Boltzmann constant, and T is the absolute temperature. From the equation (5.1), thermal activation energy is estimated to be 15.6 meV which this value is very close to the reported binding energy (16 meV) of the neutral acceptor bound exciton [17], which supports the assignment. Thus at high temperatures, eA_0 emission from native acceptor is the nonradiative centers due to thermal activation energy in temperature dependence CL spectra.

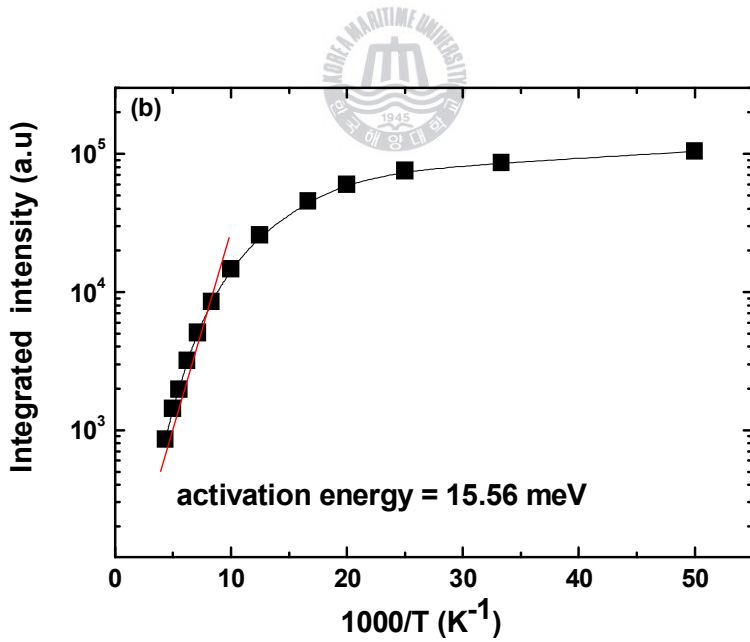
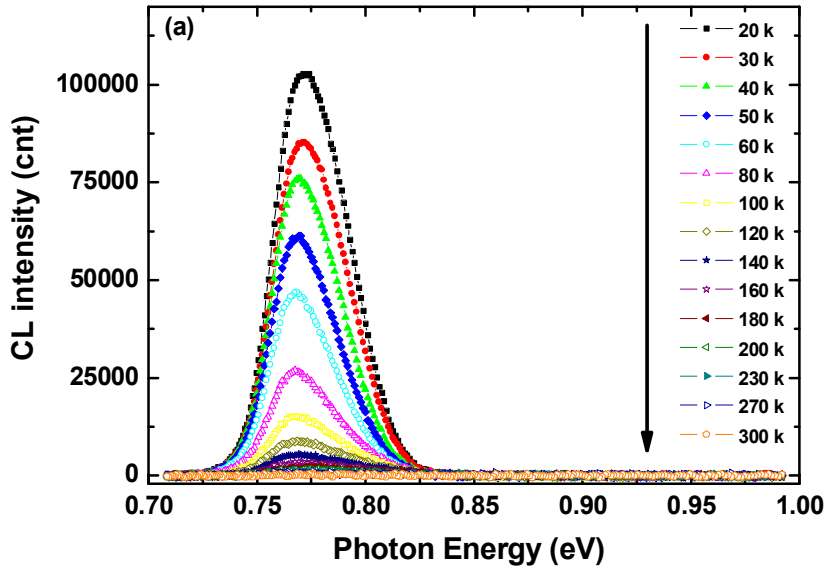


Figure 5.6 (a) temperature dependence CL spectra and (b) activation energy of eA_0 emission.

5.9) Accelerating voltage dependence CL properties

The depth profiling was by varying the accelerating voltage of the incident electron beam, different electron penetration depth can be obtained. The accelerating voltage is varied from 5 to 10 kV, which corresponds to the penetration depth of 275 nm to 876 nm deduced by Kanaya and Okayama model [17]:

$$R_e = (27.6A / \rho Z^{0.889}) V_{acc}^{1.67} \text{ (nm)} \quad (5.2)$$

where V_{acc} is an accelerating voltage in kV, A is the atomic weight in g/mol, ρ is g/cm³, and Z is the atomic number. The exciton power is kept at 3.5 nA throughout the entire study to maintain a constant generation rate of electron-hole pair [18].

This low power can minimize the radiation damage produced by the electron beam.

IN fact, negliable physical damage and luminescence intensity variation is observed on the surface of the films after the measurement. Therefore, changes in the CL intensity of the depth profiling can determine the luminescence distribution as a function of depth. In this work, CL depth profiling is estimated to determine the affects of the heterointerface in GaSb film with Zn terminated surface.

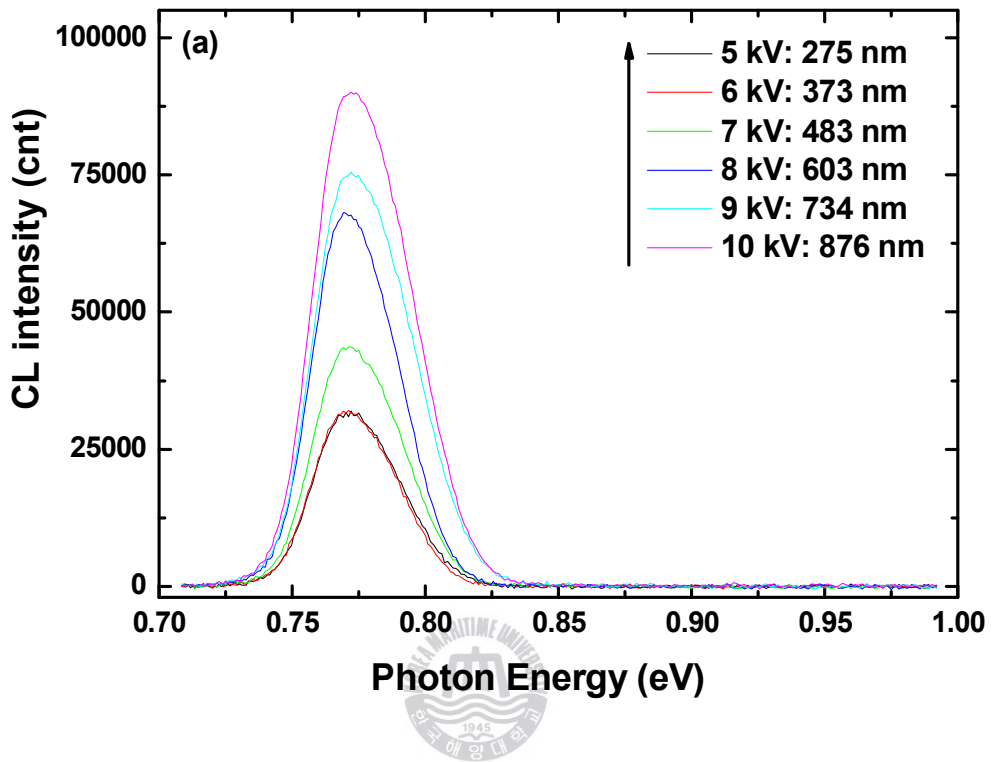


Figure 5.7 Acceleration voltage dependence CL spectra

Figure 5.7 illustrates the depth dependence of the CL spectra on the beam voltage. When the beam voltage is relatively low (5 kV ~ 6 kV) negligible variation of intensity and peak position was observed. This phenomenon is known due to dead layer. The dead layer is a surface layer which is formed due to the existence of

space-charge depletion region, and it is caused by pinning of the Fermi level by surface states [19]. As shown in figure 5.7, no obvious excitonic emission is observed for the low beam voltage of 5 ~ 6 kV, indicating that the radiative recombination is almost absent within the top dead layer. In this case, for the small incident voltage, the effect of surface recombination is dominant, reducing the pair density near the surface and leading to lower total level of excitation.

However, the emission increases rapidly as increasing the beam voltage due to the increase of excitation volume. As the penetration depth increases, the loss due to surface recombination diminishes, especially for large bulk recombination, and thus, the luminescence intensity is increased. On the other hand, from 8 kV to 9 kV, it shows anomalous behavior of both intensity and peak position. The increase ratio of intensity decreases and the peak position is occurred the red-shift. The decay of the intensities increase ratio implies that a part of the emissions is being reabsorbed into the epilayer. Internal absorption has been reported to affect the near band edge cathodoluminescence of GaN [20]. It not only reduces the emission intensity, but also red-shift the position of emission line. The absorption is caused by the pronounced band tail that is due to the structural disorder such as the

inhomogeneous strains as well as extended and point defects [21]. From these results of depth dependence CL spectra, it is known that the disorder or defect provides the anomalous characteristic of emissions. If the intensity decreases at high excitation energy over 9 kV, it can be attributed to the nonradiative recombination of minor carriers within the interface. In this work, the intensity increases over 9 KV. Therefore, this strongly suggests that the Zn-terminated ZnTe buffer layer does not make the interface.

5.10) Conclusion



The MBE of GaSb films grown on ZnTe buffer layers have been studied. GaSb films were grown on two distinct surfaces of ZnTe and the influence of surface chemical composition of ZnTe surface on the morphology and structural properties of GaSb film has been investigated. 2D growth of GaSb layer is obtained on Zn-terminated surface consequently smooth morphology and high crystal quality are achieved. The GaSb film grown on Zn-terminated ZnTe surface reveals narrow linewidth along with small residual strain. Also its luminescence properties show that eA_0 emission dominates at the low temperature cathodoluminescence spectra.

Temperature dependence of emission shows thermal activation of eA_0 emission. Moreover, from the acceleration voltage dependence, considerable feature originated from the GaSb/ZnTe has not been observed presumably due to high interface quality, which strongly supports the availability of ZnTe buffer for GaSb growth.



Reference

- [1] S. Miwa, K. Kimura, L.H. Kuo, T. Yasuda, T. Yao, Appl. Surf. Sci. 117/118 (1997) 472.
- [2] F. Lu, K. Kimura, S.Q.Wang, Z.Q. Zhu, T. Yao, J. Cryst. Growth 184/185 (1998) 183.
- [3] L.H. Kuo, K. Kimura, T. Yasuda, S. Miwa, C.G. Jin, K. Tanaka, T. Yao, Appl. Phys. Lett. 68 (1996) 2413.
- [4] S. Miwa, K. Kimura, T. Yasuda, L.H. Kuo, S. Jin, K. Tanaka, T. Yao, Appl. Surf. Sci. 107 (1996) 184.
- [5] Kanaya K, Okayama S, J. Phys. D 53 (1996) 16425
- [6] K. Akahane, N. Yamamoto, S. Gozu, N. Ohtani, J. Cryst. Growth 264 (2004) 21.
- [7] T. Yao, F. Lu, M.W. Cho, K.W. Koh, Z. Zhu, L.H. Kuo, T. Yasuda, A. Ohtake, S. Miwa, K. Kimura, K. Nakajima, K. Kimura, Phys. Status Solidi (b) 202 (1997) 657.
- [8] K. Toyoura, H. Tsujimura, T. Goto, K. Hachiya, R. Hagiwara, Y. Ito, Thin Solid Film 492 (2005) 88.
- [9] M.J. Kanstner, R. Duschl, W. Gebhardt, Microelectron. Eng 43/44 (1998) 707.



- [10] J.C. Phillips, Bonds and Bands in semiconductors, Academic Press, 1973 ch2, p. 21.
- [11] K.-N. Tu, J.W. Mayer, L.C. Feldman, Electronic Thin Film Science, Macmillan Publishing Company, 1992 ch5, pp. 103–126.
- [12] G. Bauer, W. Richter, Optical Characterization of Epitaxial Semiconductor Layers, Springer-Verlag, 1996 ch6, p 310.
- [13] B. Mendez, P.S. Dutta, J. piquerras, E. Dieguez, Appl. Phys. Lett. 67 (1995) 2648
- [14] Y.J. van der meulen, J. Phys. Chem. Solids 28 (1967) 25
- [15] D.J. Nicholas, M. Lee, B. Hamilton and K.E. Singer, J. Crys, Grow. 81 (1987) 298
- [16] J.C. Kim, H. Rho, L.M. Smith, H.E. Jackson, S. Lee, M. Dobrowolska and J.K. Furdyna, Appl. Phys. Lett. 75 (1999) 214
- [17] Kanaya K, Okayama S, J. Phys. D 53 (1996) 16425
- [18] K. Fleischer, M. Toth, M.R. Phillips, J. Zou, G. Li, and S.J. Chua, Appl. Phys. Lett. 74 (1999), 1114
- [19] J.D. Ye, H. Zhao, W. Liu, S.L. Gu, R. Zhang, Y.D. Zheng, S.T. Tan, X.W. Sun,

G.Q. Lo and K.L. Teo, Appl. Phys. Lett. 92 (2008) 131914

[20] K. Lnobloch, P. Perlin, J. Krueger, E.R. Weber and C. Kisielowski, MRS
internet J. Nitride Semicond, Res. 3 (1998) 4

[21] H.C. Ong, A.S.K. Li, G.T. Du, Appl. Phys. Lett. 78 (2001) 2667



Chapter 6. Summary and conclusions

GaSb is very useful materials for IR applications due to the narrow bandgap energy, however, the high quality GaSb growth has been restricted due to the large lattice mismatch to conventional substrate such as GaAs and InP. Therefore ZnTe buffer layer was suggested for the growth of a high-quality GaSb layer since ZnTe ($L_C = 6.104 \text{ \AA}$) has a very close lattice constant to GaSb ($L_C = 6.095 \text{ \AA}$), it is regarded as one of the best buffer layer for GaSb growth.

For the high quality ZnTe buffer, in the chapter 3, the role of low temperature ZnTe buffer layer was investigated for the high quality ZnTe buffer layer. XRD reciprocal space mapping results show structural deformation of ZnTe layer reduced by using LT-buffer and the role of LT-buffer layer is found to be the following: the reduction of misfit dislocation generation and the diminishment of the structural deformation in the overgrown layer due to the fast misfit relaxation during the growth of LT-buffer.

In the chapter 4, by using the three-step ZnTe buffer, smooth surface morphology, narrow rocking curve linewidth and the reduction of residual strain in

the GaSb layer have been achieved. It is concluded that the ZnTe buffer layer is really effective for the accommodation of the misfit to grow high-crystalline GaSb layer.

In the chapter 5, GaSb films were grown on two distinct surfaces of ZnTe and the influence of surface chemical composition of ZnTe surface on structural and optical properties of GaSb film has been investigated. The GaSb film grown on Zn-terminated ZnTe surface reveals narrow linewidth along with small residual strain and it shows the eA_0 emission at cathodoluminescence spectra. Moreover, from the acceleration voltage dependence,  considerable feature originated from the GaSb/ZnTe has not been observed presumably due to high interface quality. These results strongly support the availability of ZnTe buffer for high quality GaSb growth.

In conclusion, High crystal-quality GaSb heteroepitaxy layers are obtained by MBE. Novel ZnTe buffer layer has been introduced to growth high quality GaSb films, and the feasibility of Zn-terminated three-step ZnTe buffer layer has been demonstrated. These demonstrations indicate that ZnTe buffer layer will facilitate the growth of high quality GaSb films for the various applications in IR wavelength.

Acknowledgements

I hope to express my sincere gratitude and appreciation to Prof. Jiho Chang for his continuous encouragement and supervision. His guide is really helpful and it leads me to study. Also his coaching supports my life. I will never forget his teaching.

I would like to thank to Prof. Hongseung Kim for the critical comments and advise on this work. Also I thank to Prof. Min Yang, Prof. Hyeoungsu Ahn, Prof. Hongchan Lee and Ms. Bongchun Lee.

In this work, many people gave me assistance in Japan National Institute for Materials Science (NIMS). I really appreciate for the comments and criticism from Prof. Takashi Sekiguchi. Also I want to thank to Fukumoto san and Kamei san for her help during the six month. And I appreciate to Kumagai san, Chen Jun san, Chen bin san, Benjamin san, Wang san, Sakuma san, Fukata san, Irokawa san, and Takase san.

I especially thank to Dr. Junseok Ha, Dr. Hyojong Lee, Seunghwan Park, Hyeounjae Lee, Jinsub Park, and Koike Kayo in Tohoku university. In Tohoku university, I received many help from them.

I should also thank to Myeounghun Jung, Siyeoung Kim, and Seongkuk Choi for the discussions on MBE growth as my coworker, senior, junior, and friend. Also I thank to my laboratory member as Mina Jung, Kwanghee Kim, Jinwoo Jung, Sinae Kim, Seungjun Oh, Jinyeop Yu, Miyeoun Ju, Jieun Ku, and Youngji Cho for the assistance and reinforcement.

Special thanks should be presented to my friend, senior, junior as Bochul Chang, Jaewon Hwang, Hyeounwoo Lee, Sanghyeoun Hong, Changeun Song, Duheyoun Lee, in my university.

Finally, I am grateful to me lovely family, providing every support for me to continue studying. Their trust really becomes strong support for me.

I want to express all help and thanks from all people who support through this thesis.

CURRICULUM VITAE

October 24, 2008

PERSONAL BRIEF

Name: Last name: **Woong**, Family name: **Lee** (李雄, 이 웅)

Date of Birth: 18. Mar. 1981

Nationality: Republic of Korea

Sex: Male (single)

Address: 208-102 Dong Hyundai APT, Dadae-2 Dong, Saha-ku, Busan, 604-756,

Korea

Affiliation: Major of Nano Semiconductor, Korea Maritime University

Position: Master course student, Department of Nano semiconductor

Office Address: Dongsam-dong 1, Youngdo-ku, Busan, 606-791, Korea

Tel: +82-51-410-4833, Fax: +82-51-410-4833

E-mail: woonglee@hhu.ac.kr



EDUCATION

1997. 3 ~ 2000.2

Dae Dong High school, Pusan, Korea

2000. 3 ~ 2007. 2

B.S. in Semiconductor Physics, Korea Maritime University, Korea,

Thesis: 'Improvement of the crystallinity of MBE grown ZnTe epilayers by low-temperature buffer layer'

2007. 3 ~ Now

Master course student, Department of Nano Semiconductor, Graduate school, Korea Maritime University, Korea



MILITARY SERVICE

2001.2 ~ 2003.4

Republic of Korea Army (sergeant discharge)

ACADEMIC ACTIVITIES

2005.11 ~ 2007. 2

Research student in Nano Material and Device Laboratory,

Research Topic: Molecular Beam Epitaxy growth and characterization
of
compound semiconductors.

2007. 3 ~ Now

Master course student in Department of Applied Science, Korea
Maritime
Univ.

Research Topic: GaSb-ZnTe growth by Molecular Beam Epitaxy and
characterization



2008. 01 ~ 2008. 07

Researcher in National Institute for Materials Science, Tsukuba, Japan.
Research Topic: The investigation of Optical characterization and
morphology by SEM & CL

PUBLICATIONS

W. Lee, M. H. Jung, M. N. Jung, H. C. Lee, S. H. Park, T. Yao, J. S. Song, H. J.

Ko, J. H. Chang, Structural deformation reduction of ZnTe heteroepitaxial layers

grown on GaAs(001) substrates by using ZnTe low-temperature-buffer, **Journal of Crystal Growth**, 2007, vol 304, 22-25

W. Lee, S. Y. Kim, S. G. Choi, H. C. Lee, S. T. Lee, S.H. Park, T. Yao, J. S. Song, H. J. Ko, J. H. Chang, Molecular Beam Epitaxy of GaSb layers on GaAs(001) substrates by using three-step ZnTe buffer layers, **Journal of Crystal Growth**, 2007, vol 305, 40-44

W. Lee, S. Y. Kim, S. G. Choi, H. C. Lee, S. T. Lee, S.H. Park, T. Yao, J. S. Song, H. J. Ko, J. H. Chang, Thin film growth of GaSb layers by using three-step buffer layers, **Journal of the Research Institute of Industrial Technology**, 2007, vol. 24

W. Lee, S.Y. Kim, J.S. Song, H.J. Ko, T. Yao, Y.R. Cho, H.C. Lee, S.T. Lee, B.H. Koo, J. H. Chang, Molecular Beam Epitaxy of GaSb layers on ZnTe/GaAs: Influence of the chemical composition of ZnTe surface. **Applied Surface Science**, 2008, vol 254, 7728-7732

S. Y. Kim, **W. Lee**, M. N. Jung, H. C. Lee, S. T. Lee, Y. R. Cho, J. H. Chang , A
Study on the GaSb Thin Films Grown on ZnSe/ZnTe Superlattice Buffer Layers,
Journal of the Research Institute of Industrial Technology, 2008. vol. 25

S. Y. Kim, **W. Lee**, M. N. Jung, H. C. Lee, S. T. Lee, Y. R. Cho, J. H. Chang,
GaSb Thin Films Grown on ZnSe/ZnTe Superlattice Buffer Layers, **Sae Mulli**,
2008. vol. 56, 266



PRESENTATIONS IN INTERNATIONAL CONFERENCES

2006.08 : **W.Lee**, M.N. Jung, J.S. Song, H.J. Ko, T. Yao, J.H. Chang,
“Improvement of the crystallinity of MBE grown GaSb epilayers by using ZnTe
two-step buffer layer”, Poster presentation in Jeju-island in Korea. (ISPSA 2006)

2006.09 : **W. Lee**, M.H. Jung, H.C. Lee, S.H. Park, T. Yao, J.S. Song, H.J. Ko,
J.H. Chang, “MBE growth of high quality GaSb layers on GaAs(001) substrates
using two-step ZnTe buffer layer”, Poster presentation in Waseda univ. in Japan.

(MBE 2006)

2006.11 : S.Y. Kim, **W. Lee**, S.G. Choi, H.C. Lee, S.T. Lee, J.S. Song, T. Yao, J.H. Chang, “Improvement of the Crystallinity of MBE Grown GaSb Epilayers by Using Three-Step $ZnSe_{1-y}Te_y$ Buffer Layers”, Poster Presentation in Pusan in Korea. (Asia Nano 2006)

2006.11 : S.G. Choi, **W. Lee**, S.Y. Kim, J.H. Chnag, H.C. Lee, S.T. Lee, Y.R. Cho, “Molecular Beam Epitaxial Growth of Chalcogen Nanostructures”, Poster Presentation in Pusan in Korea. (Asia Nano 2006)

2007. 09: S.G. Choi, S.Y. Ha, M.N. Jung, S.H. Ha, **W. Lee**, H.C. Lee, Y.R. Cho, T. Yao, J.H. Chang, “Growth of well-aligned ZnO Nanorods on ITO Glass and its Application to Field Emission Device”, Poster Presentation in Jeju in Korea. (II-VI 2007)

2007. 09: S.H. Ha, M.N. Jung, S.Y. Ha, S.G. Choi, S.J. Oh, **W. Lee**, H.C. Lee,

Y.R. Cho, Y.J. An, T. Yao, J.H. Chang, “Evaluation of the Various ZnO Based Nano-Crystals for the Application to FED”, Poster Presentation in Jeju in Korea.

(II-VI 2007)

2007. 09: **W. Lee**, S.Y. Kim, H.C. Lee, S.T. Lee, T. Yao, J.S. Song, H.J. Ko, J.H. Chang, “Investigation of GaSb/ZnTe heterointerface formation”, Poster Presentation in Jeju in Korea. (II-VI 2007),

2007. 09: S.Y. Kim, **W. Lee**, M.N. Jung, H.C. Lee, S.T. Lee, J.S. Song, H.J. Ko, T. Yao, J.H. Chang Poster Presentation in Jeju in Korea. (II-VI 2007), “Molecular Beam Epitaxy of ZnSe/ZnTe Superlattice Buffer Layers for the Growth of Antimonides Thin Film”, Poster Presentation in Jeju in Korea. (II-VI 2007)

2007. 11: **W. Lee**, S.Y. Kim, H.C. Lee, S.T. Lee, Y.R. Cho, J.S. Song, H.J. Ko, T. Yao, J.H. Chang, “Molecular Beam Epitaxy of GaSb on ZnTe/GaAs – Influence of the chemical composition of ZnTe surface”, Poster Presentation in Toyko in

Japan. (ACSIN-9 2007)

2007. 11: S.Y. Kim, **W. Lee**, M.N. Jung, H.C. Lee, S.T. Lee, Y.R. Cho, J.S. Song, H.J. Ko, T. Yao, J.H. Chang, “Molecular Beam Epitaxy of ZnSe/ZnTe Superlattice Buffer Layers for the Growth of GaSb thin Film on GaAs substrate”, Poster Presentation in Seoul in Korea. (MRS 2007)

2008. 04: S.Y. Kim, **W. Lee**, J.Y. Yu, M.N. Jung, S.T. Lee, H.C. Lee, S.H. Park, D.C. Oh, T. Yao, J.H. Chang, “Enhancement of Hall mobility of Te-doped GaSb films grown on ZnTe buffer layer by Molecular Beam Epitaxy” , Poster Presentation in Daejeon in Korea. (Korea physics society 2008)

2008. 04: A.K. Nyi, S.Y. Kim, **W. Lee**, S.H. Park, D.C. Oh, T. Yao, S.T. Lee, H.C. Lee, J.H.Chang, “Temperature dependent Hall-effect measurement of Molecular Beam Epitaxial grown GaSb:Te thin Films”, Poster Presentation in Daejeon in Korea. (Korea physics society 2008)

2008. 10: **W. Lee**, M.N. Jung, J.S. Park, I.H. Im, T. Minegushi, Y. Murakami, N. Ohtsu, T. Hanada, M.W. Cho, T. Yao, T. Sekiguchi, J.H. Chang, “The X-ray photoelectron spectroscopy study of CrN surface grown for the polarity control of ZnO film”, Poster Presentation in Matsue in Japan. (VASSCAA-4)

2008. 10: **W. Lee**, S.H. Park, S.Y. Kim, H.C. Lee, S.T. Lee, J.S. Song, T. Sekiguchi, J.H. Chang, “Cathodoluminescence investigation of GaSb thin films grown on ZnTe buffer layer”, Poster Presentation in Matsue in Japan.

(VASSCAA-4)



2008. 10: S.Y. Kim, **W. Lee**, A.K. Nyi, D.C. Oh, S.H. Park, H.C. Lee, J.H. Chang, “The role of ZnTe buffer on the electrical properties of n-type GaSb:Te films”, Poster Presentation in Matsue in Japan. (VASSCAA-4)

REWARD

2005. 01 ~ 2006. 12

Awarded a scholarship student in Sewon foundation of scholarship and

culture in Korea

2007. 04

Awarded an excellent paper prize by the research institute of industrial
Technology in Korea

2007. 12

Awarded an Pusan Future Scientist prize by the Pusan metro city &
Pusan Science technology society in Korea



2008.01 ~ 2008. 07

Awarded a international cooperation research by Korea research
Foundation in Korea

EXPERIENCE OF EQUIPMENTS

Molecular Beam Epitaxy (II-VI and III-V systems); Operation and maintenance,
Growth of thin films, RHEED analysis

Vacuum thermal Evaporator; Operation, deposition,

E-beam Evaporator; Operation, deposition

High resolution X-ray diffraction measurement system; Operation, Data analysis

Atomic force microscopy; Operation, Data analysis

Scanning electron microscope; Operation. Data analysis

Cathode luminescence; Operation, Data analysis

